# *Chapter 4*

**Chapter 4**

# Design, Synthesis and Characterization of Piperidine Based Novel Derivatives for Choline Acetyltransferase Inhibitory Activity

## 4.1. Introduction

It is evident from the literature that AD is one of the most alarming neurodegenerative disorders becoming more prevalent in the current times, affecting the central nervous system and leading to the hindered cognition affecting people worldwide and the numbers of affected people are ever rising leading to a serious economic and social burden (1, 2). Piperidine is one of the most prevalent ring systems containing a nitrogen which can be found in a wide range of small-molecule drug compounds approved by FDA, having a wide range of therapeutic action like anticancer, antiviral, antimicrobial, antimalarial, antifungal, antihypertensive, anti-Alzheimer's, analgesic and antipsychotic to name few (3, 4). Also, the presence in the naturally occurring substances having therapeutic relevance makes it an integral scaffold for the drug discovery and development process (5). With the context of AD, piperidine scaffold displayed promising results with wide range of target inhibition of factors contributing to AD pathophysiology. The most prominent drug, Donepezil, a piperidine ring containing FDA approved drug used for the treatment of AD by inhibiting the AChE (6, 7).

With the above context, AD diagnostics is no different and continuously evolving with the discovery of newer and novel biomarker as well as novel compounds displaying promising activity (8). We have previously identified a novel piperidine ring containing hit compound B4 displaying promising ChAT inhibitory activity with $K_i$ value of ~11.9µM and $IC_{50}$ value of ~16.5µM at substrate concentrations ranging from 20 to 80µM were observed (9). Motivated from the findings of this previous report and also the findings of the mechanism of ChAT inhibition by the PPIs chapter 3 (Study 1), in this chapter, we explored the piperidine ring of

the previously identified hit B4 in order to simplify the structure with an objective to get a more novel, potent and selective ChAT inhibitor having a good pharmacokinetic parameters and optimal blood brain barrier permeability.

### 4.2. Objective

The objectives of this study are as follows:

- **Compound synthesis and characterization:** To synthesize different piperidine substituted amide derivatives and determine their structural properties through NMR spectroscopy and mass spectrometry.
- **In vitro ChAT inhibition assay:** To investigate the potential of synthesized derivatives as potential ChAT inhibitors assessing its inhibition. Also, to understand the selectivity of the compounds they were tested against two off-targets AChE and BuChE.
- **Physicochemical evaluation of hit compounds:** To ensure that the hit compounds meet the necessary physicochemical criteria for effective drug candidates, considering their solubility as crucial factors in drug development.
- **In vitro cytotoxicity assay:** To perform the in vitro cytotoxicity assay for the purpose of assessing the cytotoxic properties of specific hit molecules.
- **In vivo studies on rat:** To evaluate the impact of the most potent hit compound we carried out motor coordination, pharmacokinetic and brain kinetic tests.
- **In silico studies:** To perform molecular docking against ChAT followed by molecular dynamics simulation to evaluate the binding mode of the hit compound with the target protein.

## 4.3. Results and Discussion

### 4.3.1. Rationale of the design

Motivated from one of our previously reported works where we have screened a commercial library and identified some novel hits with good ChAT selective inhibitory activity. Here we have aimed to investigate the previously identified hit B4 to explore its piperidine scaffold and simplify the overall structure of the compound in order to get novel lead compound with superior selectivity and improved ChAT inhibitory activity along with optimum pharmacokinetic parameters with good blood brain barrier permeability. Here we tried substituting various aliphatic amines at the $R_1$ position and various substituted benzoic acid scaffold at the $R_2$ position (**Figure 4.1**).

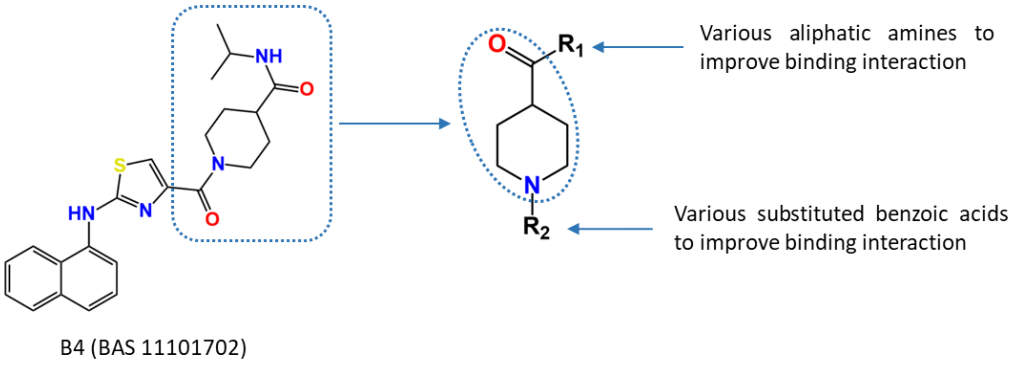


**Figure 4.1. Rationale of the synthetic scheme**

### 4.3.2. Chemistry

The starting material intermediate-1 was synthesized from isonipecotic acid by protecting the amine group of the piperidine ring with Boc anhydride, reaction takes place in the presence of water ($H_2O$) and potassium carbonate ($K_2CO3$) at room temperature as illustrated in **Scheme 4.1**. The obtained intermediate-1 is then subjected to amide coupling with various aliphatic amines ($R_1$) in the presence of 1-(3-Dimethylaminopropyl)-3-ethylcarbodiimide hydrochloride (EDC), 1-Hydroxybenzotriazole (HoBT) and triethyl amine (TEA) at room temperature overnight producing the intermediate-2. The Boc protection at the amine group of the piperidine ring is then removed from the intermediate-2 by adding 5ml, 40% trifluro acetic acid (TFA) in

DCM at room temperature for one hour giving the intermediate-3. Subsequently in the final step of the reaction various substituted benzoic acids are introduced ($R_2$) and undergoes second amide coupling reaction in the presence of EDC, HoBT and TEA at room temperature overnight producing final series of compounds A1 to A52 as illustrated in **Scheme 4.2** and **Table 4.1**, which was further purified using column chromatography.

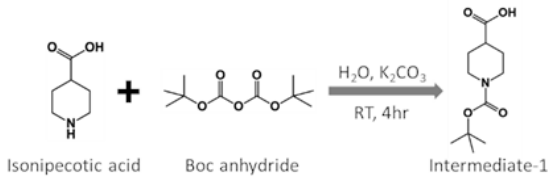


**Scheme 4.1. Synthesis of the starting material in first step.**

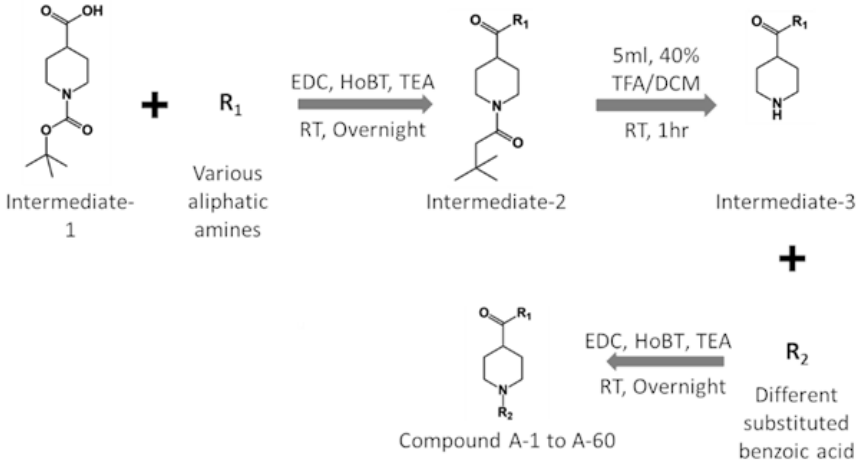


**Scheme 4.2. Synthesis of the final compounds A1 to A52**

**Table 4.1. Structure of the synthesized piperidine based derivatives A1 to A52**

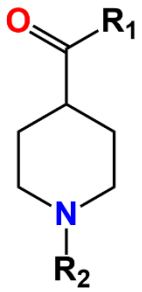


| Compound ID | $R_1$ | $R_2$ |
|---|---|---|
| A1 | Isopropyl amine | 3-Nitrobenzoic acid |

| | | |
|---|---|---|
| A2 | Isopropyl amine | 4-Bromobenzoic acid |
| A3 | Isopropyl amine | 4-Chlorobenzoic acid |
| A4 | Isopropyl amine | 3-Iodobenzoic acid |
| A5 | Isopropyl amine | 3-Chlorobenzoic acid |
| A6 | Isopropyl amine | 3-Bromobenzoic acid |
| A7 | Isopropyl amine | 4-Chloro-3-nitrobenzoic acid |
| A8 | Isopropyl amine | 3,4,5-Trimethoxybenzoic acid |
| A9 | Butylamine | 3-Nitrobenzoic acid |
| A10 | Butylamine | 4-Bromobenzoic acid |
| A11 | Butylamine | 4-Chlorobenzoic acid |
| A12 | Butylamine | 3-Iodobenzoic acid |
| A13 | Butylamine | 3-Chlorobenzoic acid |
| A14 | Butylamine | 3-Bromobenzoic acid |
| A15 | Butylamine | 4-Chloro-3-nitrobenzoic acid |
| A16 | Butylamine | 4-Nitrobenzoic acid |
| A17 | Butylamine | 3,4,5-Trimethoxybenzoic acid |
| A18 | tert-Butylamine | 3-Nitrobenzoic acid |
| A19 | tert-Butylamine | 4-Bromobenzoic acid |
| A20 | tert-Butylamine | 4-Chlorobenzoic acid |
| A21 | tert-Butylamine | 3-Iodobenzoic acid |
| A22 | tert-Butylamine | 3-Chlorobenzoic acid |
| A23 | tert-Butylamine | 3-Bromobenzoic acid |
| A24 | tert-Butylamine | 4-Chloro-3-nitrobenzoic acid |
| A25 | tert-Butylamine | 4-Nitrobenzoic acid |

| | | |
|---|---|---|
| A26 | tert-Butylamine | 3,4,5-Trimethoxybenzoic acid |
| A27 | Isopropyl amine | Benzoic acid |
| A28 | Isopropyl amine | 4-Methoxybenzoic acid |
| A29 | Isopropyl amine | 3,4-Dimethoxybenzoic acid |
| A30 | Butylamine | Benzoic acid |
| A31 | Butylamine | 4-Methoxybenzoic acid |
| A32 | Butylamine | 3,4-Dimethoxybenzoic acid |
| A33 | tert-Butylamine | 4-Methoxybenzoic acid |
| A34 | tert-Butylamine | 3,4-Dimethoxybenzoic acid |
| A35 | Diethyl amine | 3-Nitrobenzoic acid |
| A36 | Diethyl amine | 4-Bromobenzoic acid |
| A37 | Diethyl amine | 4-Chlorobenzoic acid |
| A38 | Diethyl amine | 3-Iodobenzoic acid |
| A39 | Diethyl amine | 3-Chlorobenzoic acid |
| A40 | Diethyl amine | 3-Bromobenzoic acid |
| A41 | Diethyl amine | 4-Chloro-3-nitrobenzoic acid |
| A42 | Diethyl amine | 4-Nitrobenzoic acid |
| A43 | Diethyl amine | 3,4,5-Trimethoxybenzoic acid |
| A44 | Diethyl amine | Benzoic acid |
| A45 | Diethyl amine | 4-Methoxybenzoic acid |
| A46 | Diethyl amine | 3,4-Dimethoxybenzoic acid |
| A47 | Propylamine | 3-Nitrobenzoic acid |
| A48 | Propylamine | 4-Bromobenzoic acid |
| A49 | Propylamine | 4-Nitrobenzoic acid |

| | | |
|---|---|---|
| A50 | Propylamine | 3,4,5-Trimethoxybenzoic acid |
| A51 | Propylamine | 4-Methoxybenzoic acid |
| A52 | Propylamine | 3,4-Dimethoxybenzoic acid |

### 4.3.3. *In vitro* ChAT inhibition screening assay of the synthesized compounds A1 to A52

The synthesized compounds (**A1 to A52**) were screened for their activity against human recombinant ChAT using our in-house high throughput fluorometric assay, at a single final concentration of 100 µM (**Figure 4.2**) in a sextuplicate runs in six different plates and the averages of six plates are shown. Tenatoprazole, one of the PPIs that has been reported by us as a potent ChAT inhibitor was used as a positive control. At the 100 µM concentration, tenatoprazole inhibited ChAT activity by 98.8%.

The in-vitro activity screening indicated that the compound A1 was the best inhibitor of human rChAT with 87.87% inhibition of the enzyme activity (**Figure 4.2A**). Also, various other compounds A37 to A52 were found to have good inhibitory potential but due to the interpolate variation A1 was considered to be the best with the most potency and least interpolate variation. The synthesized compounds were also screened against two of the off-targets, namely BuChE and AChE (**Figure 4.2B and 4.2C, respectively**) in a sextuplicate run in a single plate, in order to determine the selectivity of the compounds for ChAT. Eserine a dual ChE inhibitor was used for the positive control, inhibited both BuChE and AChE by 100%. The results indicated that most of the compounds were having negligible inhibition on the off-targets. Compound A1 displayed no inhibitory activity on BuChE and 26.62% inhibition of AChE, thus, was identified to be the best performing compound with highest selectivity for ChAT inhibition.

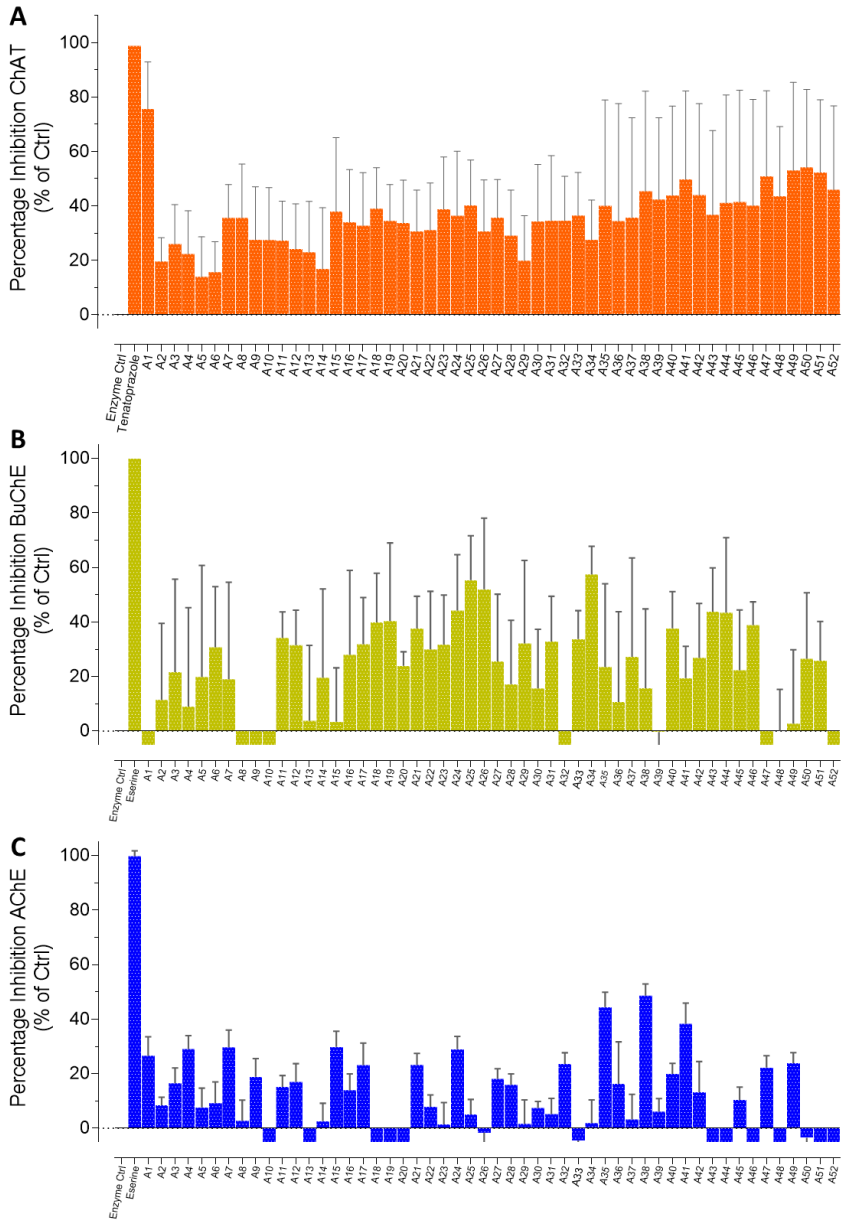


**Figure 4.2. Screening of synthesized compounds for ChAT, AChE and BuChE enzymes inhibition. A**) Percentage inhibition of rChAT by the synthesized compounds at 100 µM concentration. Tenatoprazole was used as a positive control and a well without inhibitor containing 0.2% DMSO was used as enzyme control indicating 100 % enzyme activity. **B)** and **C)** Represent the percentage inhibition of BuChE & rAChE by the synthesized compounds, respectively. Eserine was used as a positive control and a well without inhibitor containing 0.2% DMSO was used as enzyme control indicating 100 % enzyme activity. The data is presented as mean ± SD of an individual experiments performed in sextuplicate. The compound with over

70% inhibition were selected for further kinetic analysis. rChAT = recombinant choline acetyltransferase; rAChE = recombinant acetylcholinesterase; BuChE = butyrylcholinesterase.

### 4.3.4. ChAT inhibition kinetics analyses provided the inhibition constant and the modeof inhibition for A1

From the initial in-vitro screening it was indicated that the compound A1 was the best performing among the synthesized series of compounds having the best ChAT inhibitory activity with negligible off-target effects. We hence proceeded to perform the full ChAT inhibition kinetic assessment for the compound A1. The inhibition constant ($K_i$) and the $IC_{50}$ values are shown in **Figure 4.3** for A1, calculated based on the dose response curves at wide concentration range of the compound and choline as the enzyme substrate. The 2D structure of the compound A1 is shown in (**Figure 4.3A**). A1 exhibited a $K_i$ value of 20.36 µM which was estimated by nonlinear regression analysis of the whole dataset (**Figure 4.3B**). The $IC_{50}$ value was 31.08 µM at substrate concentrations ranging between 18 to 300 µM (**Figure 4.3D**). Nonlinear regression statistic suggested that A1 is a mixed-competitive inhibitor of ChAT because its data was fitted best in a mixed model inhibition equation. This was confirmed with Lineweaver-Burk plot (double reciprocal) analyses of the substrate-velocity curves of the rChAT enzyme activity at different substrate concentrations (ranging from 1.56 to 25 µM) with or without inhibitors at specified concentrations (**Figure 4.3C**). The Lineweaver-Burk plots were fitted using the linear regression analysis function of GraphPad Prism 9 software. Reciprocal of rate (1/v) is plotted as a function of reciprocal of substrate concentration (1/S) for various concentrations of A1, which produced straight lines on the graph where the X- and Y-axis intercept represents $-1/K_m$ and $1/V_{max}$, while the slope is represented by $K_m/V_{max}$. The Lineweaver-Burk plot indicated that the $K_m$ value increases, and the $V_{max}$ value decreases with increasing A1 concentrations, suggesting a mixed model type inhibition of ChAT by A1, in line with the nonlinear regression analyses of the data. The $K_m$ and $V_{max}$ values for all concentrations

of A1 were also calculated using the substrate-velocity curves (**Figure 4.3B**), which are presented in (**Table 4.4**).

**Table 4.2.** The $K_m$ and $V_{max}$ values for compound A1 at different concentrations, obtained from the ChAT inhibition kinetic analysis performed using GraphPad Prism 7.

| Compound | Concentration (µM) | $V_{max}$ (µM /min) | $K_m$ (µM) | R square |
|---|---|---|---|---|
| **A1** | 0 | 31169 | 108.9 | 0.9894 |
| | 1.56 | 28940 | 101.7 | 0.9920 |
| | 3.13 | 30864 | 123.1 | 0.9915 |
| | 6.25 | 31256 | 119.5 | 0.9872 |
| | 12.5 | 29034 | 133.3 | 0.9920 |
| | 25 | 25092 | 144.5 | 0.9942 |
| | 50 | 15050 | 177.3 | 0.9813 |
| | 100 | 7599 | 226.9 | 0.7495 |

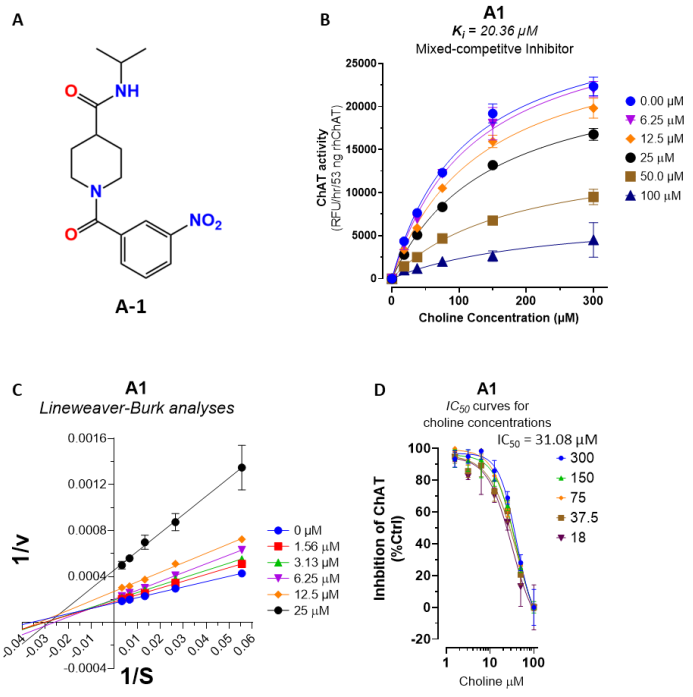


**Figure 4.3. ChAT Inhibition Kinetic for compound A1**. **A)** Molecular structure of compound A1. **B)** Non-linear regression fitting of the data and the estimated inhibition constant ($K_i$) within the wide range of the substrate concentrations (x-axis) and the A1 concentration range of 6.25

to 100μM. The analysis was done by fitting and statistically comparing the data based on four different equations in GraphPad Prism 9, namely competitive, non-competitive, uncompetitive and mixed-competitive models. The result indicated that A1 data fitted best as the mixed-competitive inhibition mode of activity compared to all the other models (all $p<0.001$). **C)** The Lineweaver-Burk plot analysis for confirmation of the mode of action of A1 as inhibitor of ChAT. The plot was obtained from the substrate-velocity curves of the ChAT enzyme activity at different substrate concentrations and the specified concentration range of A1 (i.e., from 1.56 to 25 μM). The Lineweaver-Burk plots were fitted using the linear regression analysis function of GraphPad Prism 9 software. **D)** Dose-response curves for estimation of $IC_{50}$ of A1 against ChAT at the specified substrate concentrations. The $IC_{50}$ value was calculated after fitting the curves using nonlinear regression function of GraphPad Prism 9. ChAT = recombinant choline acetyltransferase.

### 4.3.5. In Vitro Cytotoxicity Assay

We assessed the effect of compound A1 on SH-SY5Y neuroblastoma cell to evaluate its cytotoxicity using MTT assay, given that potential tracers must be non-toxic compounds. The test was performed at two different concentrations of 10 μM and 50 μM. The data, expressed as percent cell viability indicated that compound A1 had no significant toxic effect on the viability of the cells (**Figure 4.4**). Treatments were performed for 24 h. The percentages cell viability for A1 at 10 μM and 50 μM concentrations were 93.70 ± 7.42 % and 104.73 ± 18.71 % respectively. Furthermore, the morphological changes of the SH-SY5Y cells were observed under the inverted light microscope (**Figure 4.5**) which indicated no cell damage occurred at the given tested concentration of A1, thus providing crucial information about the safety of our compound under investigation.

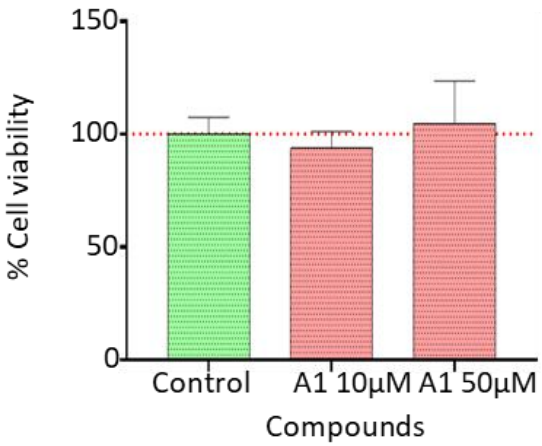


**Figure 4.4.** Cellular toxicity analyses for A1 using the human neuroblastoma cell line, SH-SY5Y cells. The analyses were done using MTT cell viability test. The cells were exposed for 24 hours to the 10 and 50 µM final concentrations of the compounds. Data are expressed as % mean values ± SD of 6 readings. Viability of the vehicle treated control cells were considered as 100%.

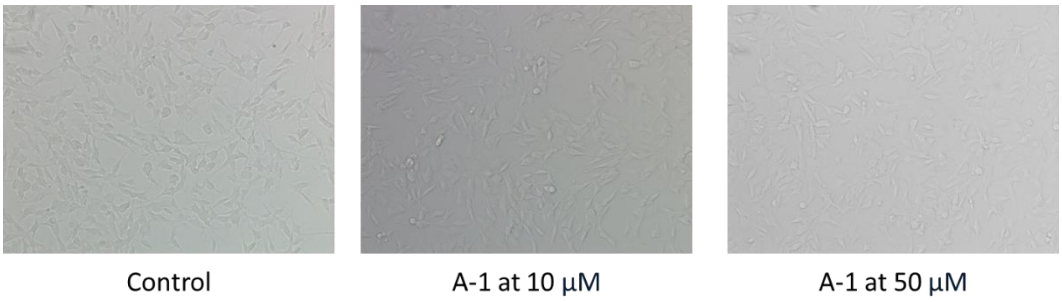


**Figure 4.5.** Morphological changes of SH-SY5Y cells as observed under an inverted light microscope (Nikon ECLIPSE TE300, 20× magnification).

### 4.3.6. Solubility and percentage purity analysis of the Hit Compound

The solubility of drug candidates plays a pivotal role in context to drug discovery, ensuring an effective administration and absorption within the body. It has been observed that many potent lead compounds do not progress to clinical trial stages due to their reduced bioavailability, which is often a consequence of inadequate solubility. Given our ultimate goal is to develop the identified compounds as in vivo biomarkers for ChAT-containing targets in the brain, an

optimal balance between the hydrophilicity and lipophilicity will be the key to obtain good pharmacokinetic profiles. Calibration curve was prepared beforehand (**Figure 4.6A**) to quantify the kinetic solubility studies for the compound A1 and the $R^2$ value for the obtained calibration curve was found to be 0.9976, indicating the robustness of the HPLC methodology. It revealed that the solubility for A1 was 0.12 mg/ml. This suggests that at pH 7.4, compound A1 exhibit good solubility. Percentage purity calculations were also carried out for the compounds at 100 µM concentrations, which are shown as chromatogram in (**Figure 4.6B**). The purity was found to be 96.94 %.

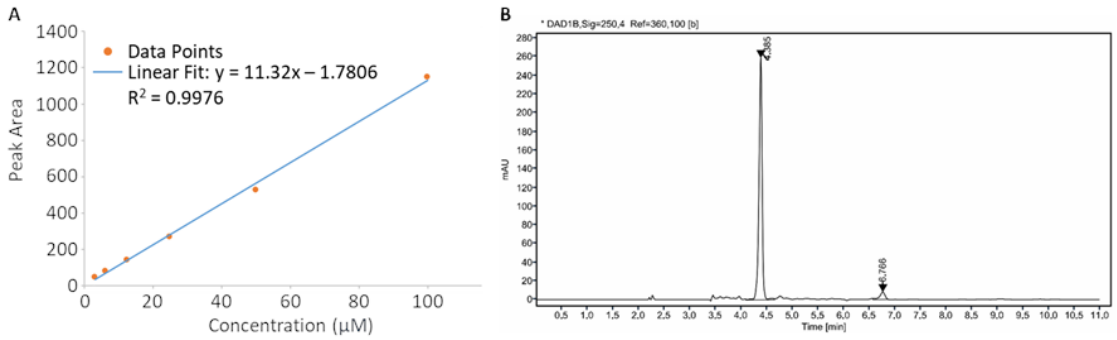


**Figure 4.6.** Solubility and percentage purity of A1 : HPLC: Agilent 2004, Column Specification Poroshell 123, EC C18 4µm, 4.6*150mm, sample volume for each injection was 20 µl. A) HPLC calibration curve for A1 using 6 times serial dilutions of 100 µM, 50 µM, 25 µM, 12.5 µM, 6.25 µM and 3.125 µM; B) HPLC chromatogram of compound A1, where gradient and isocratic method was used, solvent system used Acetonitrile = 0-70 %: Water = 100-30 % for initial 2 minutes and continued for the next 9 minutes, Flow rate was set to 0.4 ml/min, Absorbance was recorded at 250nm.

### 4.3.7. In Vivo studies of compound A1 in Sprague-Dawley rats

#### 4.3.7.1. A1 did not affect motor coordination post i.v. administration in rats in Rotarod test

The Rotarod test is a commonly used method in neurobiology to assess motor coordination and

balance in rodents, primarily mice and rats. The test involves placing the animal on a rotating rod and measuring how long it can stay on the rod without falling. The rats were trained for 20 to 30 minute every day for three consecutive day and on the 4$^{th}$ day of compound A1 administration at 10 mg/kg i.v., effect of the compound on motor coordination was tested 1 hr post administration and the results indicated that the A1 didn't show any effect on motor coordination of the rats (**Figure 4.7**).

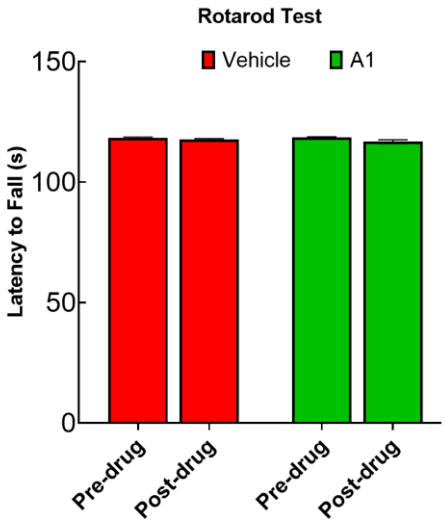


**Figure 4.7. A1 did not affect motor coordination in SD rats.** A1 administration in normal healthy SD rats showed no sign of motor incoordination in the rotarod test. Data were expressed as Mean ± SEM and analyzed by two-way ANOVA (Tukey's multiple comparisons) (n=6). Red indicates the vehicle group and green indicates the test group administered A1. A1 doses (10mg/kg i.v.).

### 4.3.7.2. In-vivo pharmacokinetic study of compound A1

Rat pharmacokinetic model was used and two different route of administration was selected intra venous (i.v.) and per oral (p.o.) along with three different dosages of A1: 1, 5, 10 mg/kg body weight for both the routes of administration (**Table 4.3)**. Animals were distributed into six groups and n=6 in each group. Blood samples were collected and were proceeded according

to the methodology discussed and the plasma samples were then processed and the levels of A1 was quantified using HPLC.

**Table 4.3. In-vivo pharmacokinetic animal distribution.**

| S.No | Group | No of animals | Group |
|---|---|---|---|
| 1 | A1_oral | 6 | 1 mg/kg of lead compound 1 by oral administration |
| 2 | A1_Oral | 6 | 5 mg/kg of lead compound 1 by oral administration |
| 3 | A1_Oral | 6 | 10 mg/kg of lead compound 1 by oral administration |
| 4 | A1_i.v. | 6 | 1 mg/kg of lead compound 1 by i.v. administration |
| 5 | A1_i.v. | 6 | 5 mg/kg of lead compound 1 by i.v. administration |
| 6 | A1_i.v. | 6 | 10 mg/kg of lead compound 1 by i.v. administration |
| **Total animals** | | **36** | |

Finally, the pharmacokinetic parameters were calculated and the graph was plotted (**Figure 4.8**), which indicated that the compound A1 have an optimum pharmacokinetics. The resultant pharmacokinetic parameters are shown in **Table 4.4**, where it can be observed that the pharmacokinetic properties remained constant with the different dosage and also there was a slight improvement with the increased dose. The $t_{1/2}$ of the compound A1 was found to improve with increased dosage from 1.78 h at 1mg/kg i.v. administration to 2.76 h at 5mg/kg i.v. administration and subsequently at 10mg/kg i.v. administration it was observed to be around 3.4 h. The $T_{max}$ is the time needed to reach maximum concentration, since it was a single i.v. bolus dose and the first sample drawn post drug administration was at 0.5 h thus it shows $T_{max}$ at 0.5 h. The maximal concentration of the compound A1 was found to be around 50-60 % of the drug administered which indicated that the drug is distributing to the body. The mean

residence time (MRT) indicating the average time for the compound A1 stays in the body was observed to be 2.5, 3.9, 4.7 hrs respectively at dosage of 1, 5, 10 mg/kg, and is dose dependent higher the dosage better the MRT was observed. The observed clearance (Cl_obs) of A1 was low which indicated that the compound might be going to the various organ tissues. Also, the terminal elimination rate constant (Lambda_z) value was calculated give in **Table 4.4** indicates that the compound has a moderate elimination rate. We did not get any HPLC signal from the plasma samples collected from animals administered through oral route, thus, not able to quantify the data for the oral administration. This might be due to the compound contains two amide bonds and might be getting metabolized and broken down in the gastro intestinal tract or may be getting first pass metabolized post absorption by the liver.

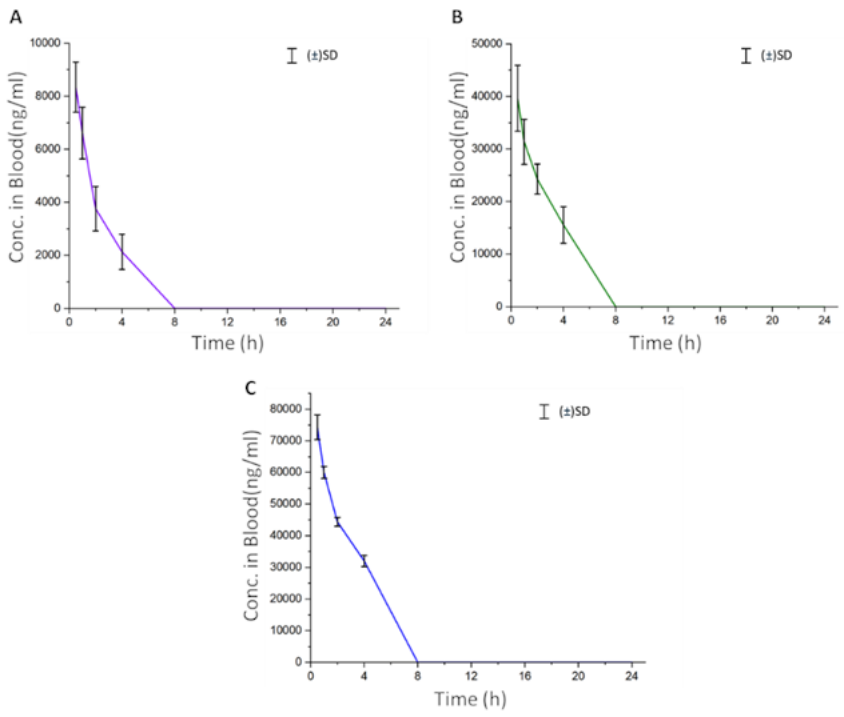


**Figure 4.8. Concentration in plasma for A1 obtained from in vivo pharmacokinetic study.** A) A1 administered at 1 mg/kg i.v.; B) A1 administered at 5 mg/kg i.v.; C) A1 administered at 10 mg/kg i.v. The result obtained was the average of the three readings taken and the error bars are shown as the Standard deviation (SD).

**Table 4.4. in-vivo pharmacokinetic parameter estimation.**

| Parameter | Unit | Final value ± SD | | |
|---|---|---|---|---|
| | | **1 mg/kg i.v.** | **5 mg/kg i.v.** | **10 mg/kg i.v.** |
| Lambda_z | 1/h | 0.3969 ± 0.0743 | 0.2593 ± 0.0595 | 0.2067 ± 0.0295 |
| $t_{1/2}$ | h | 1.7853 ± 0.3138 | 2.7628 ± 0.5965 | 3.4033 ± 0.053 |
| $T_{max}$ | h | 0.5 | 0.5 | 0.5 |
| $C_{max}$ | ng/ml | 8351.149 ± 942.505 | 39634.667 ± 6261.944 | 74294 ± 3883.399 |
| $C_0$ | ng/ml | 10558.66 ± 824.59 | 50749.78 ± 13002.29 | 92375.72 ± 12437.18 |
| AUC 0-t | ng/ml*h | 19552.35 ± 3178.301 | 108018.44 ± 5630.2178 | 203864.8471 ± 3048.6659 |
| AUC 0-inf | ng/ml*h | 25229.99 ± 4332.437 | 171323.47 ± 25823.5081 | 361807.25 ± 35789.1226 |
| MRT | h | 2.5217 ± 0.4786 | 3.92357 ± 0.91352 | 4.7886 ± 0.6764 |
| Cl_obs | (mg/kg)/(ng/ml)/h | 0.00004 ± 0.00001 | 0.00003 ± 0.000005 | 0.000028 ± 0.000003 |
| $V_d$ | (mg/kg)/(ng/ml) | 0.0001 ± 0.00002 | 0.00011 ± 0.00001 | 0.000132 ± 0.000005 |

### 4.3.7.3. In-vivo brain kinetic study of compound A1

Furthermore, in a different setup in vivo brain kinetics study was performed in order to determine the BBB permeability of the compound and to check whether the compound reaches the brain post administration. Since development of AD diagnostics primarily targets the brain, the brain kinetic profile was quantified using HPLC and the graph was plot (**Figure 4.9**) and the kinetic parameters were estimated given in **Table 4.5**. From the graph it can be observed that the compound reaches the brain significantly nearly up to 20-25 % of the total drug administered with $T_{max}$ of 1 h, having a half life $t_{1/2}$ of 5.44 h, which indicates that the compound A1 retains more in the brain tissues which also correlates to the higher MRT of 7.96 h. The Lambda_z value of 0.1284 $h^{-1}$ indicates a moderate elimination which indicates a good window

of time post administration and the compound reaching the target tissue, thus, could be beneficial if developed as imaging marker compounds for ChAT, for cholinergic neuronal health. We have further analyzed the data to calculate the Targeting index of the compound which was found to be 1.245, the value greater than 1 indicates that our drug potentially reaches to the brain tissues at the intended biologically relevant site, this finding can also indicate that the compound would show minimum unintended interactions or off-target effects, which can be correlated to the optimized efficacy and safety profile of the compound A1.

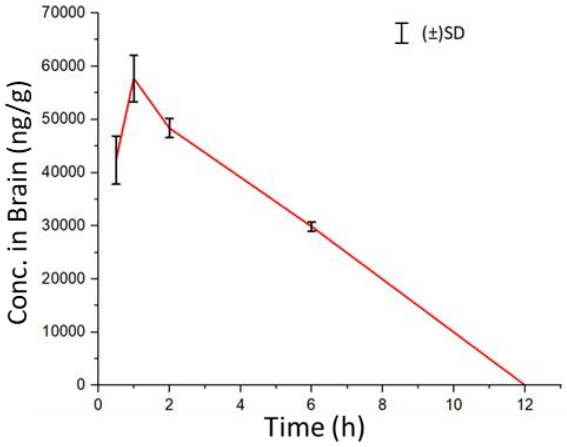


**Figure 4.9. Concentration in brain for A1 obtained from in vivo brain kinetic study.** A1 administered at 10 mg/kg i.v. The result obtained was the average of the three readings taken and the error bars are shown as the Standard deviation (SD).

**Table 4.5. in-vivo brain kinetic parameter estimation.**

| Parameter | Unit | Final value ± SD |
|---|---|---|
| Lambda_z | 1/h | 0.1284 ± 0.0142 |
| $t_{1/2}$ | h | 5.44 ± 0.57 |
| $T_{max}$ | h | 1 |
| $C_{max}$ | ng/g | 57713.57 ± 4383.23 |
| $C_0$ | ng/g | 42357.2 ± 4524.304 |
| AUC 0-t | ng/g*h | 255683 ± 5127.02 |

| | | |
|---|---|---|
| AUC 0-inf | ng/g*h | 490182.32 ± 23506.012 |
| MRT | h | 7.96 ± 0.8 |
| Cl_obs | (mg/kg)/(ng/g)/h | 0.00002 ± 0.000001 |
| $V_d$ | (mg/kg)/(ng/ml) | 0.000162 ± 0.000009 |
| Targeting Index | - | 1.254 |

### 4.3.8. In Silico Molecular Docking Study

Docking study was carried out to understand the binding mode of interaction of the compound A1 in the ChAT binding tunnel, from the **Figure 4.10A** it can be observed that the nitro group present on the aromatic benzene ring of the compound A1 lies in close proximity to the HIS324 and seems to have a van der waals interaction with it during the docking, along with it the piperidine ring seems to be stabilizing the conformation by having a Pi-Alkyl interaction with the ILE330 amino acid residue, and the other surrounding residues play a crucial role in stabilizing the A1 compound in the binding tunnel by having a van der waals and formation of carbon hydrogen bond and the docking score was found to be -7.4 kcal/mol. We also docked α-NETA (**Figure 4.10B**) as a standard compound a known ChAT inhibitor, with a docking score of -6.8 kcal/mol and it seems the naphthalene ring interacts with the HIS324 by formation of PI-PI T-shaped bond, along with it also the VAL449 interacts with the ring system via a Pi-alkyl bond formation. And the quaternary nitrogen seems to interact with the TYR552 via a Pi-cation bond formation. These findings indicate that the compound A1 has a higher binding affinity towards the ChAT binding tunnel as compared to the standard α-NETA.

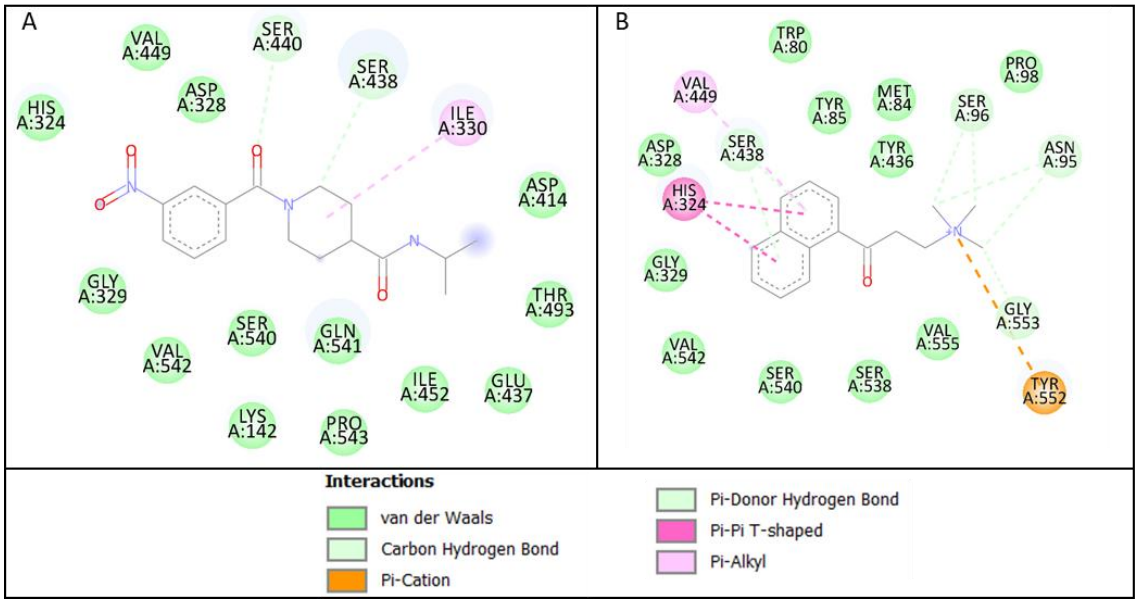


**Figure 4.10. 2D docking interaction diagram.** A) For compound A1; B) For standard α-NETA.

### 4.3.9. Molecular Dynamics Simulation Study

We also carried out classical molecular dynamic's simulation of the hit compound A1 to understand the crucial dynamics of the binding mechanism with ChAT binding tunnel, the structural changes that might take place and contribute to the overall stability of the formed complex with respect to time. The input for the MD simulation were taken from the results obtained in docking study.

Primarily the obtained trajectories of the complexes were evaluated for their RMSD value. At first the ChAT protein RMSD was observed that formed complexes with α-NETA and A1 (**Figure 4.11A**), where the blue and green line represents the ChAT protein in the complex system with α-NETA and A1 respectively. The protein RMSD value was observed between 0.15 to 0.28 nm for both complexes, reaching equilibrium within the first 10 ns and was stable throughout the simulation without any significant changes during the simulation time. The ChAT protein RMSD for the complex with hit compound A1 was slightly lower as compared

to the standard compound α-NETA indicating better compatibility of the compound A1 with the ChAT binding tunnel and denoting better folding process during the complex formation. Similarly, we evaluated the ligand RMSD for α-NETA and A1 (**Figure 4.11B**) and the values ranged between 0.2 to 0.6 nm and 0.3 to 0.5 nm respectively, indicating good range of flexibility of the ligands in the binding pocket of the ChAT, where compound A1 had a better RMSD range as compared to α-NETA which displayed some uncertain jump in RMSD values during the simulation indicating that the compound A1 has a better compatibility in the ChAT binding tunnel.

Furthermore, the RMSF of the obtained trajectories were evaluated to elucidate the presence of any uncertain fluctuations or the overall flexibility of the system necessary for the complex formation process. The protein RMSF value (**Figure 4.11C**) was observed in the range between 0.1 to 1.2 nm for both the ChAT_α-NETA and ChAT_A1 complexes. The graphs illustrate a sharp peak for the N-terminus (residue ~0), indicating high flexibility at this part of the protein sequence, most likely due to a high exposure of the N-terminal surface with the solvent. Overall, the protein RMSF plot indicated that the ChAT protein was rigid in most of the regions which was due to its quaternary folding and the regions of the binding tunnel was having optimal flexibility from 100-200 and 300-400 indicated by its higher RMSF value in the plot. Likewise, ligand RMSF value (**Figure 4.11D**) was observed in the range of 0.02 to 0.25 nm indicating good amount of flexibility necessary for the ligand to fit well within the binding tunnel of the ChAT.

Next, we also evaluated the RoG of the simulated complexes (**Figure 4.11E**) and was in the range of 2.51 to 2.55 nm for both the standard ChAT_α-NETA complex and the ChAT_A1 complex. Both the systems exhibited stable folding process with minor fluctuations, suggesting that the ChAT protein retained its quaternary structure and overall shape during the complex

formation process and was consistent throughout the simulation indicating good stability of the formed complex. Next, we analyzed the HBN for the formed complex, where for the ChAT_A1 complex (**Figure 4.11F**) maintained 1 to 3 H-bonds during the simulation time as compared to the standard ChAT_α-NETA complex (**Figure 4.11G**) which maintained only 1 H-bond during the simulation, indicating better interaction of the A1 with the ChAT binding tunnel. Also, the HBD was calculated for the complex systems (**Figure 4.11H**) where it can be seen that the optimal H-bond distance was maintained below 0.3 nm which indicated strong H-bonding. Furthermore, we also performed the SASA analysis for the trajectories under investigation in order to understand how the SASA of the hydrophobic core of the ChAT protein changes upon complex formation with the ligands. We observed that the SASA for the ChAT_A1 complex (**Figure 4.11I**) the protein SASA was higher in the range of 255 to 267 $nm^2$ and on complex formation with A1 the SASA values were slightly reduced and was in the range of 252 to 265 $nm^2$. Similarly, for the standard ChAT_α-NETA complex (**Figure 4.11J**) the ChAT protein SASA was higher in the range of 257 to 270 $nm^2$ and on complex formation SASA was slightly reduced and was found to be in the range of 252 to 266 $nm^2$. This finding indicates that the interaction of the compound A1 with the ChAT binding tunnel stabilized the hydrophobic core leading to the slightly reduced and more stable SASA and was comparable with the standard α-NETA.

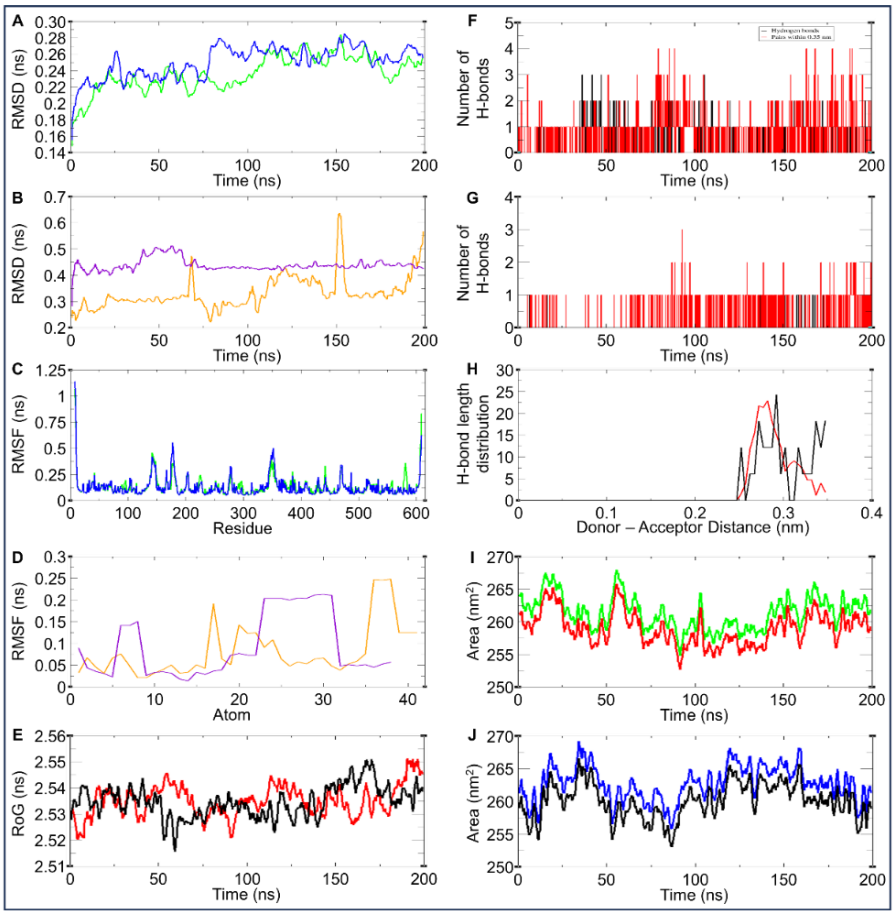


**Figure 4.11. Comparative analysis for the 200 ns simulated MD trajectories of ChAT_α-NETA as reference and ChAT_A1 complex** A) RMSD plots for the ChAT protein during formation of a complex with α-NETA (blue) and formation with A1 (green). B) RMSD plot for α-NETA (orange) and A1 (purple) during the simulation. C) RMSF landscape for ChAT protein during its complex formation with α-NETA and A1 throughout the simulation. D) RMSF plot α-NETA (orange) and A1 (purple) during their complex formation with ChAT protein. E) RoG plot for ChAT_α-NETA complex (black) and ChAT_A1 complex (red). F) Number of H-bond formed within the ChAT_A1 complex. G) Number of H-bond formed within the ChAT_α-NETA complex. H) Average distance maintained by the formed H-bonds between ChAT_α-NETA complex (black) and ChAT_A1 complex (red). I) The changes in SASA values of the ChAT_A1 complex (red) in comparison to the ChAT protein alone (green). J) The changes in SASA values of the ChAT_α-NETA complex (black) in comparison to the ChAT protein alone

(blue).

We also carried out PCA analysis for the systems, where initially the eigenvector index was plotted with respect to eigenvalues to understand the components that contribute to the maximum motion, (**Figure 4.12A**) The graph illustrates that the contribution of the eigenvalues decreases rapidly from the first eigenvector index to the second and the continuous decline is seen followed to each subsequent eigenvector. Indicating that the first two principal components account for the most significant motion of the systems under investigation. Finally, the first two principal components were used for further analysis (**Figure 4.12B**). The ChAT_α-NETA and ChAT_A1 complexes both displayed similar essential dynamics having a widespread distribution in the graph where each dots represents a significant motion undergone by the system during complex formation, indicating that the conformational transitions were happening in a stable and controlled manner during the 200 ns MD simulation without any abrupt motion or uncertainties. Finally, we also performed the FEL analysis, where the ChAT_α-NETA and ChAT_A1 complexes displayed in **Figure 4.12C and 4.12D** respectively indicates a narrow and centralized single funnel formation with a distinct centralized low energy region (blue color) indicates that the complex reached its energy minima conformation in a stable process.

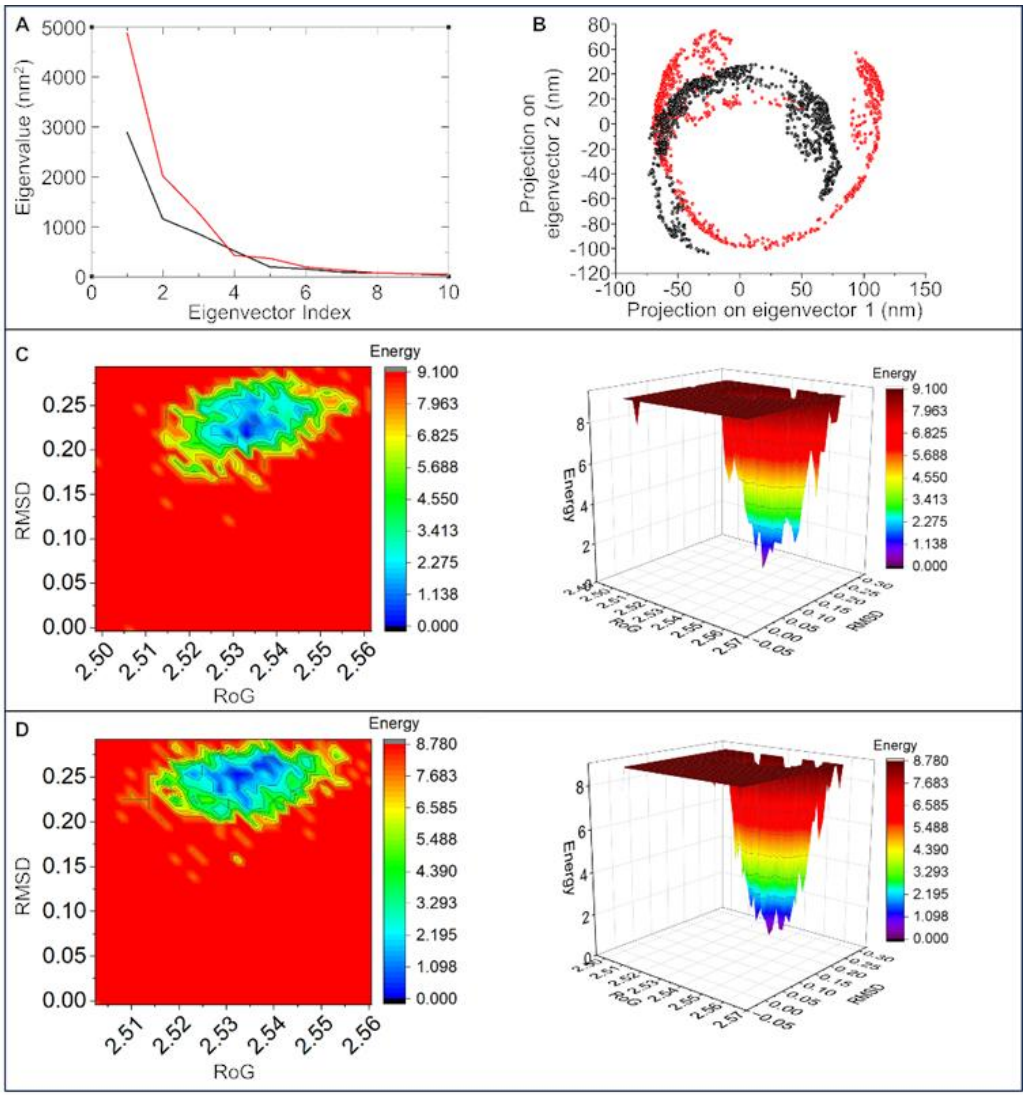


**Figure 4.12.** PCA and FEL analysis of the obtained trajectories A) Eigenvalue calculation for the first 10 principal components for ChAT_α-NETA complex (black) and ChAT_A1 complex (red). B) PCA for the first two PCs for the simulated systems ChAT_α-NETA (black) and ChAT_A1 (red) C-D) The 2D and 3D plot representations of FEL analysis for ChAT_α-NETA and ChAT_A1, respectively.

### 4.4. Materials and Methods

#### 4.4.1. Chemistry

All the reagents and chemicals used for the synthesis and characterization of compounds were purchased from Sigma-Aldrich, Alfa-Aesar, and SRL (Sisco Research Laboratories Pvt. ltd). The solvents were dried by standard solvent drying methods. The compounds were

characterized by AVH D 500 AVANCE III HD 500 MHz OneBay NMR Spectrometer at IITBHU, and High-resolution mass spectra (HRMS) were obtained by electrospray (HRMS/ESI), recorded with Agilent1100 LC-Q-TOF and HRMS-6540-UHD machine at Department of Chemistry, Banaras Hindu University. All the structures were drawn by using ChemDraw Ultra. For sample quantification, we used RP-HPLC Agilent 1260 infinity II. The NMR, HRMS spectra of all the compounds is given in **Annexure I (page no. 233 to 292).**

#### 4.4.1.1. General procedure for the synthesis of Boc protected isonipecotic acid (Intermediate-1)

Isonipecotic acid was used as the starting compound for the synthesis where initially in the first step of the reaction the amine group of the piperidine moiety of the isonipecotic acid was protected by using Di-tert-butyl decarbonate (Boc anhydride), where isonipecotic acid was dissolved in water with 2 eq of $K_2CO_3$ and on the other hand Boc anhydride 1 eq was dissolved in Tetrahydrofuran (THF) as a solvent. The aqueous mixture was put in ice bath at 0°C and was put on a magnetic stirrer, and with time dropwise addition of the THF solution of Boc anhydride was done, after the addition of the two solvent phase reaction mixture was allowed to slowly reach to the room temperature and the reaction was allowed to continue for 4 hours, followed by which workup was done by evaporating the THF using a rotary evaporator, and addition of 2-3 ml of diethyl ether was done , followed by the addition of dil. HCL to reduce the pH of the reaction mixture to pH 2 which resulted in precipitation of the intermediate-1. Which was then extracted with ethyl acetate using a separating funnel and dried using rotary evaporator for further use.

#### 4.4.1.2. General procedure for the synthesis of Piperidine Based amide substituted compounds (A1 to A52)

The intermediate-1 was taken in the second step where 1.3 eq of EDC was added and dissolved

in Dichloromethane (DCM) as solvent quantity sufficient, followed by the addition of 1.3 eq of HoBT and the resultant mixture was allowed to dissolve and put under ice bath at 0°C. Finally, 3 eq of Triethylamine was added to the mixture and at the end various different aliphatic amines 1 eq were added as per the reaction. The reaction was slowly allowed to reach room temperature and then kept for overnight followed by which the reaction mixture was forwarded for workup to get the intermediate-2 using a separating funnel and DCM was used to extract the intermediate-2. In the third step the Boc protection was removed from the amine of the piperidine ring of the intermediate-2 by the help of 5ml, 40% TFA in DCM and was kept in stirring for 1 h, followed by which the TFA was evaporated using rotary evaporator, giving the intermediate-3. In the final forth step of the reaction the various different substituted benzoic acids were taken as per the reaction and 1.3 eq of EDC was added and dissolved in DCM as solvent quantity sufficient, followed by the addition of 1.3 eq of HoBT and the resultant mixture was allowed to dissolve and put under ice bath at 0°C. Finally, 3 eq of Triethylamine was added to the mixture and at the end the intermediate-3 was added to the reaction and the reaction was allowed for overnight, followed by workup where the final resultant compound was separated using DCM in a separating funnel, and was further purified using the silica gel column chromatography [100−200], eluent: ethyl acetate/n-hexane] to obtain the pure product.

**4.4.1.2.1**. **N-isopropyl-1-(3-nitrobenzoyl)piperidine-4-carboxamide** (**A1**)

**$^{1}$H NMR (500 MHz, $CDCl_3$)** δ 8.31 – 8.20 (m, 2H), 7.73 (d, *J* = 7.6 Hz, 1H), 7.61 (t, *J* = 7.9 Hz, 1H), 5.39 (d, *J* = 6.6 Hz, 1H), 4.67 (s, 1H), 4.05 (dt, *J* = 27.0, 13.5 Hz, 1H), 3.72 (s, 1H), 3.02 (d, *J* = 82.1 Hz, 2H), 2.46 – 2.12 (m, 1H), 1.87 (d, *J* = 64.8 Hz, 4H), 1.14 (d, *J* = 6.6 Hz, 6H). **$^{13}$C NMR (126 MHz, $CDCl_3$)** δ 172.54, 167.59, 147.96, 137.44, 132.80, 129.71, 124.34, 121.97, 47.08, 42.86, 41.74, 41.23, 29.55, 28.39, 22.63, 13.97. **HRMS (ESI):** *m/z* calculated for $C_{16}H_{21}N_3O_4$ $[M+H]^+$: 320.1610; found : 320.1586.

**4.4.1.2.2**. **1-(4-bromobenzoyl)-N-isopropylpiperidine-4-carboxamide** (**A2**)

**$^{1}$H NMR (500 MHz, $CDCl_3$)** δ 7.34 (dd, *J* = 21.1, 8.6 Hz, 4H), 5.39 (d, *J* = 7.0 Hz, 1H), 4.64 (s, 1H), 4.05 (d, *J* = 20.9 Hz, 1H), 3.77 (s, 1H), 2.91 (d, *J* = 58.6 Hz, 2H), 2.38 – 2.13 (m, 1H), 1.81 (d, *J* = 68.4 Hz, 4H), 1.13 (d, *J* = 6.6 Hz, 6H). **$^{13}$C NMR (126 MHz, $CDCl_3$)** δ 172.91, 169.44, 135.78, 134.25, 128.80, 128.41, 43.20, 41.34, 29.69, 28.76, 22.77.

**4.4.1.2.3**. **1-(4-chlorobenzoyl)-N-isopropylpiperidine-4-carboxamide** (**A3**)

**$^{1}$H NMR (500 MHz, $CDCl_3$)** δ 7.56 (d, *J* = 1.9 Hz, 1H), 7.54 (s, 1H), 7.32 – 7.29 (m, 1H), 7.29 – 7.27 (m, 1H), 5.36 (d, *J* = 7.3 Hz, 1H), 4.68 (s, 1H), 4.22 – 3.95 (m, 1H), 3.79 (s, 1H), 2.94 (d, *J* = 61.0 Hz, 2H), 2.30 (t, *J* = 11.2 Hz, 1H), 1.74 (s, 4H), 1.16 (d, *J* = 6.6 Hz, 6H). **$^{13}$C NMR (126 MHz, $CDCl_3$)** δ 172.41, 168.98, 134.37, 131.32, 128.20, 123.55, 42.80, 40.90, 29.27, 28.41, 22.36.

**4.4.1.2.4**. **1-(3-iodobenzoyl)-N-isopropylpiperidine-4-carboxamide** (**A4**)

**$^{1}$H NMR (500 MHz, $CDCl_3$)** δ 7.76 – 7.71 (m, 2H), 7.36 – 7.32 (m, 1H), 7.14 (t, *J* = 7.8 Hz, 1H), 5.37 – 5.28 (m, 1H), 4.67 (s, 1H), 4.07 (dd, *J* = 13.8, 7.2 Hz, 1H), 3.80 (s, 1H), 2.93 (d, *J* = 97.4 Hz, 2H), 2.28 (tt, *J* = 11.3, 3.9 Hz, 1H), 1.72 (d, *J* = 39.3 Hz, 4H), 1.14 (d, *J* = 6.6 Hz, 6H). **$^{13}$C NMR (126 MHz, $CDCl_3$)** δ 172.84, 168.55, 138.67, 138.00, 135.65, 130.23, 125.95, 94.27, 77.30, 77.05, 76.80, 43.25, 41.34, 22.81.

**4.4.1.2.5**. **1-(3-chlorobenzoyl)-N-isopropylpiperidine-4-carboxamide** (**A5**)

**$^{1}$H NMR (500 MHz, $CDCl_3$)** δ 7.43 – 7.39 (m, 2H), 7.38 – 7.34 (m, 1H), 7.29 (d, *J* = 4.3 Hz, 1H), 5.48 – 5.20 (m, 1H), 4.68 (s, 1H), 4.21 – 3.96 (m, 1H), 3.80 (s, 1H), 2.97 (d, *J* = 67.2 Hz, 2H), 2.32 (dd, *J* = 22.8, 7.6 Hz, 1H), 1.75 (d, *J* = 51.1 Hz, 4H), 1.17 (d, *J* = 6.6 Hz, 6H). **$^{13}$C NMR (126 MHz, $CDCl_3$)** δ 172.84, 168.86, 137.69, 134.62, 129.88, 127.05, 124.95, 43.25, 41.34, 22.81.

**4.4.1.2.6**. **1-(2-bromobenzoyl)-N-isopropylpiperidine-4-carboxamide** (**A6**)

**$^{1}$H NMR (500 MHz, $CDCl_3$)** δ 7.56 (dd, *J* = 7.0, 1.2 Hz, 2H), 7.31 (dt, *J* = 7.6, 5.6 Hz, 2H), 5.26 (s, 1H), 4.77 (s, 1H), 4.01 (s, 1H), 3.77 (s, 1H), 2.94 (d, *J* = 90.5 Hz, 2H), 2.32 (d, *J* = 18.3 Hz, 1H), 1.81 (s, 4H), 1.17 (d, *J* = 6.6 Hz, 6H). **$^{13}$C NMR (126 MHz, $CDCl_3$)** δ 172.70, 168.59, 137.85, 132.61, 130.03, 129.80, 125.29, 122.55, 43.10, 41.23, 29.58, 22.67.

**4.4.1.2.7**. **1-(4-chloro-3-nitrobenzoyl)-N-isopropylpiperidine-4-carboxamide** (**A7**)

**1H NMR (500 MHz, $CDCl_3$)** δ 7.92 (s, 1H), 7.59 (t, J = 12.2 Hz, 2H), 5.31 (d, J = 12.3 Hz, 1H), 4.77 – 4.41 (m, 1H), 4.07 (d, J = 20.8 Hz, 1H), 3.66 (d, J = 44.3 Hz, 1H), 2.95 (s, 2H), 2.31 (t, J = 11.0 Hz, 1H), 1.83 (d, J = 64.7 Hz, 4H), 1.15 (d, J = 6.6 Hz, 6H). **$^{13}$C NMR (126 MHz, $CDCl_3$)** δ 172.63, 166.74, 136.36, 135.75, 132.26, 131.57, 128.43, 124.38, 120.39, 43.01, 41.40, 31.92, 29.68, 29.35, 22.73, 14.10.

**4.4.1.2.8**. **N-isopropyl-1-(3,4,5-trimethoxybenzoyl)piperidine-4-carboxamide** (**A8**)

**$^{1}$H NMR (500 MHz, $CDCl_3$)** δ 6.60 (s, 2H), 5.39 – 5.20 (m, 1H), 4.66 (s, 1H), 4.08 (dt, *J* = 14.4, 7.2 Hz, 1H), 3.89 (s, 1H), 3.85 (d, *J* = 5.4 Hz, 9H), 2.92 (s, 2H), 2.28 (d, *J* = 7.8 Hz, 1H), 1.80 (s, 4H), 1.14 (d, *J* = 6.6 Hz, 6H). **$^{13}$C NMR (126 MHz, $CDCl_3$)** δ 173.02, 170.24, 153.32, 139.02, 131.36, 104.03, 60.91, 56.25, 43.40, 41.34, 22.80.

**4.4.1.2.9**. **N-butyl-1-(3-nitrobenzoyl)piperidine-4-carboxamide** (**A9**)

**$^{1}$H NMR (500 MHz, $CDCl_3$)** δ 8.27 (t, J = 9.4 Hz, 2H), 7.75 (d, J = 10.2 Hz, 1H), 7.62 (t, J = 8.2 Hz, 1H), 5.49 (d, J = 35.9 Hz, 1H), 4.66 (s, 1H), 3.72 (s, 1H), 3.31 – 2.82 (m, 4H), 2.49 – 2.19 (m, 1H), 1.53 – 1.44 (m, 2H), 1.33 (d, J = 7.0 Hz, 2H), 1.36 – 1.15 (m, 4H), 0.97 – 0.89 (m, 3H). **$^{13}$C NMR (126 MHz, $CDCl_3$)** δ 173.42, 167.74, 148.13, 137.58, 132.94, 129.83, 124.48, 122.11, 77.26, 77.01, 76.76, 43.00, 39.28, 31.69, 20.04, 13.71.

**4.4.1.2.10**. **1-(4-bromobenzoyl)-N-butylpiperidine-4-carboxamide** (**A10**)

**$^{1}$H NMR (500 MHz, $CDCl_3$)** δ 7.55 (s, 2H), 7.28 (s, 2H), 5.61 (s, 1H), 4.62 (s, 1H), 3.74 (s, 1H), 3.37 (s, 2H), 2.97 (s, 2H), 2.31 (s, 1H), 1.75 (s, 3H), 1.38 (t, *J* = 59.7 Hz, 5H), 0.96 (s,

3H). **$^{13}$C NMR (126 MHz, $CDCl_3$)** δ 173.65, 169.40, 134.81, 131.75, 128.62, 123.98, 77.28, 77.02, 76.77, 43.17, 39.24, 31.69, 29.02 – 28.86, 20.03, 13.72.

**4.4.1.2.11**. **N-butyl-1-(4-chlorobenzoyl)piperidine-4-carboxamide** (**A11**)

**$^{1}$H NMR (500 MHz, $CDCl_3$)** δ 7.37 (d, *J* = 8.6 Hz, 2H), 7.33 (dd, *J* = 8.5, 1.8 Hz, 2H), 5.58 (s, 1H), 4.64 (s, 1H), 3.78 (s, 1H), 3.24 (dd, *J* = 10.0, 4.2 Hz, 2H), 2.92 (s, 2H), 2.40 – 2.19 (m, 1H), 1.79 (d, *J* = 55.2 Hz, 4H), 1.53 – 1.41 (m, 2H), 1.33 (d, *J* = 7.5 Hz, 2H), 0.92 (dt, *J* = 7.4, 3.6 Hz, 3H). **$^{13}$C NMR (126 MHz, $CDCl_3$)** δ 173.67, 169.38, 135.77, 134.33, 128.79, 128.42, 43.17, 39.23, 31.69, 29.68, 28.94, 20.03, 13.72. **HRMS (ESI):** *m/z* calculated for $C_{17}H_{23}BrN_2O_2$ $[M+H]^+$: 323.1526; found : 323.1504.

**4.4.1.2.12**. **N-butyl-1-(3-iodobenzoyl)piperidine-4-carboxamide** (**A12**)

**$^{1}$H NMR (500 MHz, $CDCl_3$)** δ 7.77 – 7.70 (m, 2H), 7.35 – 7.32 (m, 1H), 7.13 (t, J = 7.7 Hz, 1H), 5.60 (s, 1H), 4.65 (s, 1H), 3.76 (s, 1H), 3.27 – 3.19 (m, 2H), 2.92 (d, J = 66.9 Hz, 2H), 2.36 – 2.25 (m, 1H), 1.81 (d, J = 45.4 Hz, 4H), 1.50 – 1.43 (m, 2H), 1.34 (dt, J = 14.9, 7.4 Hz, 2H), 0.91 (t, J = 7.3 Hz, 3H). **$^{13}$C NMR (126 MHz, $CDCl_3$)** δ 173.68, 168.54, 138.64, 138.01, 135.65, 130.21, 125.93, 94.23, 43.14, 39.25, 31.69, 29.51, 29.34 – 29.21, 28.69, 20.04, 13.73. **HRMS (ESI):** *m/z* calculated for $C_{17}H_{23}IN_2O_2$ $[M+H]^+$: 415.0882; found : 415.0856.

**4.4.1.2.13**. **N-butyl-1-(3-chlorobenzoyl)piperidine-4-carboxamide** (**A13**)

**$^{1}$H NMR (500 MHz, $CDCl_3$)** δ 7.42 – 7.39 (m, 2H), 7.36 (td, *J* = 7.5, 0.9 Hz, 1H), 7.30 – 7.26 (m, 1H), 5.57 (s, 1H), 4.69 (s, 1H), 3.81 (s, 1H), 3.31 – 3.15 (m, 2H), 2.99 (d, *J* = 58.9 Hz, 2H), 2.35 (t, *J* = 11.2 Hz, 1H), 1.74 (s, 4H), 1.50 (dt, *J* = 14.8, 7.4 Hz, 2H), 1.40 – 1.30 (m, 2H), 0.94 (t, *J* = 7.3 Hz, 3H). **$^{13}$C NMR (126 MHz, $CDCl_3$)** δ 173.63, 168.83, 137.72, 134.63, 129.86, 127.05, 124.93, 77.28, 77.02, 76.77, 43.16, 39.24, 31.69, 29.68, 20.04, 13.72.

**4.4.1.2.14**. **1-(3-bromobenzoyl)-N-butylpiperidine-4-carboxamide** (**A14**)

**$^{1}$H NMR (500 MHz, $CDCl_3$)** δ 7.56 (d, *J* = 8.9 Hz, 2H), 7.37 – 7.25 (m, 2H), 5.60 (s, 1H), 4.67

(s, 1H), 3.78 (s, 1H), 3.31 – 3.22 (m, 2H), 2.96 (d, *J* = 94.4 Hz, 2H), 2.42 – 2.27 (m, 1H), 1.87 (d, *J* = 69.2 Hz, 4H), 1.54 – 1.44 (m, 2H), 1.35 (dt, *J* = 14.6, 7.4 Hz, 2H), 0.94 (t, *J* = 7.3 Hz, 3H). **$^{13}$C NMR (126 MHz, $CDCl_3$)** δ 173.67, 168.70, 137.92, 132.74, 130.19, 129.88, 125.38, 122.68, 43.20, 39.25, 31.69, 20.06, 13.77.

**4.4.1.2.15**. **N-butyl-1-(4-chloro-3-nitrobenzoyl)piperidine-4-carboxamide** (**A15**)

**$^{1}$H NMR (500 MHz, $CDCl_3$)** δ 7.94 (d, *J* = 1.9 Hz, 1H), 7.63 (d, *J* = 8.2 Hz, 1H), 7.59 (dd, *J* = 8.2, 1.9 Hz, 1H), 5.56 (s, 1H), 4.64 (s, 1H), 3.77 (s, 1H), 3.28 (dd, *J* = 10.0, 4.2 Hz, 2H), 3.01 (d, *J* = 112.7 Hz, 2H), 2.44 – 2.29 (m, 1H), 1.90 (d, *J* = 69.2 Hz, 4H), 1.49 (dd, *J* = 14.7, 7.6 Hz, 2H), 1.36 (dd, *J* = 15.2, 7.3 Hz, 2H), 0.94 (t, *J* = 7.3 Hz, 3H). **$^{13}$C NMR (126 MHz, $CDCl_3$)** δ 173.44, 166.75, 147.79, 135.70, 132.26, 131.61, 128.47, 124.41, 42.95, 39.29, 31.68, 20.05, 13.76.

**4.4.1.2.16**. **N-butyl-1-(4-nitrobenzoyl)piperidine-4-carboxamide** (**A16**)

**$^{1}$H NMR (500 MHz, $CDCl_3$)** δ 8.27 (d, J = 8.7 Hz, 2H), 7.56 (d, J = 8.7 Hz, 2H), 5.50 (s, 1H), 4.69 (s, 1H), 3.65 (s, 1H), 3.25 (dd, J = 13.0, 7.0 Hz, 2H), 3.05 (s, 1H), 2.90 (s, 1H), 2.35 (dd, J = 20.0, 6.1 Hz, 1H), 1.85 (d, J = 49.0 Hz, 4H), 1.52 – 1.42 (m, 2H), 1.38 – 1.30 (m, 2H), 0.92 (t, J = 7.3 Hz, 3H). **$^{13}$C NMR (126 MHz, $CDCl_3$)** δ 173.46, 168.03, 148.36, 142.16, 127.90, 123.96, 43.03, 39.28, 31.69, 20.05, 13.76.

**4.4.1.2.17**. **N-butyl-1-(3,4,5-trimethoxybenzoyl)piperidine-4-carboxamide** (**A17**)

**$^{1}$H NMR (500 MHz, $CDCl_3$)** δ 6.63 (s, 2H), 5.57 (s, 1H), 4.61 (s, 1H), 3.87 (d, J = 5.2 Hz, 9H), 3.27 (dd, J = 13.0, 7.0 Hz, 2H), 2.94 (s, 2H), 2.32 (s, 1H), 1.84 (d, J = 46.7 Hz, 5H), 1.42 – 1.30 (m, 3H), 0.94 (t, J = 7.3 Hz, 3H). **$^{13}$C NMR (126 MHz, $CDCl_3$)** δ 173.84, 170.24, 153.32, 139.03, 131.35, 104.08, 103.97, 60.98, 60.84, 56.32, 56.18, 43.37, 39.25, 31.69, 20.05, 13.74.

**4.4.1.2.18**. **N-(tert-butyl)-1-(3-nitrobenzoyl)piperidine-4-carboxamide** (**A18**)

**$^{1}$H NMR (500 MHz, $CDCl_3$)** δ 8.31 – 8.25 (m, 2H), 7.76 – 7.71 (m, 1H), 7.62 (t, J = 7.9 Hz,

1H), 5.31 (s, 1H), 4.67 (s, 1H), 3.72 (s, 1H), 3.02 (d, J = 82.5 Hz, 2H), 2.27 (dd, J = 20.6, 5.5 Hz, 1H), 1.94 – 1.65 (m, 4H), 1.35 (s, 9H). **$^{13}$C NMR (126 MHz, $CDCl_3$)** δ 172.94, 167.74, 148.08, 137.59, 132.92, 129.83, 124.49, 122.11, 77.30, 77.05, 76.79, 51.31, 43.63, 29.26 – 27.68.

**4.4.1.2.19**. **1-(4-bromobenzoyl)-N-(tert-butyl)piperidine-4-carboxamide** (**A19**)

**$^{1}$H NMR (500 MHz, $CDCl_3$)** δ 7.58 – 7.52 (m, 2H), 7.31 – 7.26 (m, 2H), 5.33 (d, J = 14.8 Hz, 1H), 4.68 (s, 1H), 3.77 (s, 1H), 2.98 (d, J = 107.8 Hz, 2H), 2.20 (s, 1H), 1.78 (s, 4H), 1.35 (s, 9H). **$^{13}$C NMR (126 MHz, $CDCl_3$)** δ 173.17, 169.40, 134.83, 131.75, 128.61, 123.95, 51.24, 43.82, 28.82.

**4.4.1.2.20**. **N-(tert-butyl)-1-(4-chlorobenzoyl)piperidine-4-carboxamide** (**A20**)

**$^{1}$H NMR (500 MHz, $CDCl_3$)** δ 7.41 – 7.37 (m, 2H), 7.37 – 7.33 (m, 2H), 5.34 (s, 1H), 4.69 (s, 1H), 3.77 (s, 1H), 2.95 (d, J = 83.3 Hz, 2H), 2.25 (ddd, J = 11.2, 7.6, 3.6 Hz, 1H), 1.79 (t, J = 59.3 Hz, 4H), 1.36 (s, 9H). **$^{13}$C NMR (126 MHz, $CDCl_3$)** δ 173.17, 169.40, 135.72, 134.34, 128.80, 128.42, 77.31, 77.06, 76.80, 51.25, 43.84, 28.82.

**4.4.1.2.21**. **N-(tert-butyl)-1-(3-iodobenzoyl)piperidine-4-carboxamide** (**A21**)

**$^{1}$H NMR (500 MHz, $CDCl_3$)** δ 7.81 – 7.72 (m, 2H), 7.37 (d, J = 7.6 Hz, 1H), 7.16 (t, J = 7.7 Hz, 1H), 5.31 (s, 1H), 4.68 (s, 1H), 3.80 (s, 1H), 2.92 (d, J = 100.8 Hz, 2H), 2.26 (t, J = 15.2 Hz, 1H), 1.85 (d, J = 75.2 Hz, 4H), 1.37 (s, 9H). **$^{13}$C NMR (126 MHz, $CDCl_3$)** δ 173.14, 168.57, 138.03, 135.63, 130.23, 125.94, 94.26, 51.27, 43.85, 28.83, 1.04.

**4.4.1.2.22**. **N-(tert-butyl)-1-(3-chlorobenzoyl)piperidine-4-carboxamide** (**A22**)

**$^{1}$H NMR (500 MHz, $CDCl_3$)** δ 7.42 – 7.33 (m, 3H), 7.29 (d, J = 5.0 Hz, 1H), 5.30 (s, 1H), 4.67 (s, 1H), 3.80 (d, J = 18.7 Hz, 1H), 2.94 (d, J = 93.9 Hz, 2H), 2.23 (s, 1H), 1.87 (d, J = 60.3 Hz, 4H), 1.37 (s, 9H). **$^{13}$C NMR (126 MHz, $CDCl_3$)** δ 173.12, 168.86, 137.73, 134.61, 129.87, 127.04, 124.94, 51.27, 43.84, 28.82. **HRMS (ESI):** *m/z* calculated for $C_{17}H_{23}ClN_2O_2$ $[M+H]^+$:

323.1526; found : 323.1509.

**4.4.1.2.23**. **1-(3-bromobenzoyl)-N-(tert-butyl)piperidine-4-carboxamide** (**A23**)

**$^{1}$H NMR (500 MHz, $CDCl_3$)** δ 7.58 – 7.51 (m, 2H), 7.35 – 7.27 (m, 2H), 5.33 (d, *J* = 14.0 Hz, 1H), 4.67 (s, 1H), 3.77 (s, 1H), 2.95 (d, *J* = 70.0 Hz, 2H), 2.38 – 2.17 (m, 1H), 1.75 (d, *J* = 12.4 Hz, 4H), 1.36 (s, 9H). **$^{13}$C NMR (126 MHz, $CDCl_3$)** δ 173.14, 168.68, 137.98, 132.70, 130.17, 129.87 (d, J = 5.6 Hz), 125.37, 122.66, 51.25, 43.81, 28.82. **HRMS (ESI):** *m/z* calculated for $C_{17}H_{23}BrN_2O_2$ $[M+H]^+$: 367.1021; found : 323.1509.

**4.4.1.2.24**. **N-(tert-butyl)-1-(4-chloro-3-nitrobenzoyl)piperidine-4-carboxamide** (**A24**)

**$^{1}$H NMR (500 MHz, $CDCl_3$)** δ 7.91 (d, *J* = 1.9 Hz, 1H), 7.60 (d, *J* = 8.2 Hz, 1H), 7.55 (dd, *J* = 8.2, 1.9 Hz, 1H), 5.31 (s, 1H), 4.63 (s, 1H), 3.72 (s, 1H), 3.00 (d, *J* = 105.1 Hz, 2H), 2.26 (tt, *J* = 11.1, 4.0 Hz, 1H), 1.74 (d, *J* = 2.8 Hz, 4H), 1.34 (s, 9H). **$^{13}$C NMR (126 MHz, $CDCl_3$)** δ 172.88, 166.73, 147.79, 135.76, 132.89 – 132.15, 131.57, 128.42, 124.39 (d,), 77.31, 77.06, 76.80, 51.33, 43.54, 28.81.

**4.4.1.2.25**. **N-(tert-butyl)-1-(4-nitrobenzoyl)piperidine-4-carboxamide** (**A25**)

**$^{1}$H NMR (500 MHz, $CDCl_3$)** δ 8.27 – 8.23 (m, 2H), 7.56 – 7.52 (m, 2H), 5.28 (d, J = 9.1 Hz, 1H), 4.65 (d, J = 12.5 Hz, 1H), 3.63 (d, J = 11.4 Hz, 1H), 3.08 – 2.81 (m, 2H), 2.25 (dd, J = 16.5, 9.6 Hz, 1H), 1.81 (d, J = 87.8 Hz, 4H), 1.32 (s, 9H). **$^{13}$C NMR (126 MHz, $CDCl_3$)** δ 172.94, 168.02, 148.33, 142.22, 127.87, 123.95 (d,), 51.31, 47.05, 43.61, 41.71, 29.17 – 27.35.

**4.4.1.2.26**. **N-(tert-butyl)-1-(3,4,5-trimethoxybenzoyl)piperidine-4-carboxamide** (**A26**)

**$^{1}$H NMR (500 MHz, $CDCl_3$) δ** 7.29 (s, 1H) 6.59 (s, 2H), 5.29 (s, 1H), 4.59 (s, 1H), 3.85 (d, J = 4.5 Hz, 9H), 2.91 (s, 2H), 2.22 (s, 1H), 1.72 (s, 3H), 1.34 (s, 9H), 0.84 (s, 2H). **$^{13}$C NMR (126 MHz, $CDCl_3$)** δ 173.29, 170.24, 153.31, 139.01, 131.40, 104.01, 56.25, 51.26, 44.03, 28.83, 1.03.

**4.4.1.2.27**. **1-benzoyl-N-isopropylpiperidine-4-carboxamide** (**A27**)

**$^{1}$H NMR (500 MHz, $CDCl_3$)** δ 7.39 (s, 5H), 5.35 (s, 1H), 4.71 (s, 1H), 4.12 – 3.72 (m, 2H), 2.91 (d, J = 65.8 Hz, 2H), 2.28 (t, J = 11.3 Hz, 1H), 1.74 (s, 4H), 1.14 (d, J = 1.5 Hz, 3H), 1.13 (d, J = 1.6 Hz, 3H). **$^{13}$C NMR (126 MHz, $CDCl_3$)** δ 173.01, 170.52, 135.97, 129.68, 128.53, 126.87, 43.39, 41.32, 22.81.

**4.4.1.2.28**. **N-isopropyl-1-(4-methoxybenzoyl)piperidine-4-carboxamide** (**A28**)

**$^{1}$H NMR (500 MHz, $CDCl_3$)** δ 7.35 (t, J = 5.8 Hz, 2H), 6.90 (d, J = 2.0 Hz, 2H), 5.46 (d, J = 7.3 Hz, 1H), 4.18 – 3.94 (m, 1H), 3.82 (s, 3H), 2.89 (s, 2H), 2.39 – 2.20 (m, 1H), 1.93 – 1.67 (m, 4H), 1.25 (d, J = 9.5 Hz, 2H), 1.13 (s, 3H), 1.12 (s, 3H). **$^{13}$C NMR (126 MHz, $CDCl_3$)** δ 173.10, 170.49, 160.73, 128.96, 128.04, 113.72, 77.32, 77.07, 76.81, 55.37, 43.42, 41.26, 28.93, 22.79, 1.03.

**4.4.1.2.29**. **1-(3,4-dimethoxybenzoyl)-N-isopropylpiperidine-4-carboxamide** (**A29**)

**$^{1}$H NMR (500 MHz, $CDCl_3$)** δ 6.96 (s, 2H), 6.84 (d, J = 8.6 Hz, 1H), 5.36 (s, 1H), 4.07 (dd, J = 13.3, 6.6 Hz, 1H), 3.88 (d, J = 4.6 Hz, 6H), 2.92 (s, 2H), 2.27 (t, J = 11.2 Hz, 1H), 1.77 (dd, J = 42.2, 13.0 Hz, 4H), 1.24 (s, 3H), 1.14 (d, J = 6.5 Hz, 6H). **$^{13}$C NMR (126 MHz, $CDCl_3$)** δ 173.07, 170.47, 150.28, 148.97, 128.20, 119.93, 110.63 (d, J = 18.1 Hz), 77.29, 77.04, 76.78, 55.99, 43.42, 41.31, 29.69, 28.91, 22.78.

**4.4.1.2.30**. **1-benzoyl-N-butylpiperidine-4-carboxamide** (**A30**)

**$^{1}$H NMR (500 MHz, $CDCl_3$) δ** 7.38 (d, J = 6.9 Hz, 5H), 5.55 (s, 1H), 4.67 (s, 1H), 3.77 (s, 1H), 3.25 (dd, J = 13.2, 6.3 Hz, 2H), 2.94 (d, J = 61.0 Hz, 2H), 2.32 (dd, J = 15.2, 7.4 Hz, 1H), 1.72 (d, J = 44.3 Hz, 4H), 1.51 – 1.44 (m, 2H), 1.33 (dd, J = 14.9, 7.6 Hz, 2H), 0.92 (t, J = 7.3 Hz, 3H). **$^{13}$C NMR (126 MHz, $CDCl_3$)** δ 173.79, 170.48, 136.01, 129.65, 128.51, 126.85, 43.32, 39.23, 31.70, 29.70, 20.04, 13.74.

**4.4.1.2.31**. **N-butyl-1-(4-methoxybenzoyl)piperidine-4-carboxamide** (**A31**)

**$^{1}$H NMR (500 MHz, $CDCl_3$) δ** 7.36 (d, J = 8.7 Hz, 2H), 6.89 (d, J = 7.1 Hz, 2H), 3.82 (s, 3H), 3.24 (d, J = 12.8 Hz, 2H), 2.93 (s, 2H), 2.32 (s, 1H), 1.90 – 1.67 (m, 5H), 1.49 – 1.43 (m, 2H), 1.33 (s, 3H), 0.88 (dd, J = 35.4, 15.0 Hz, 4H). **$^{13}$C NMR (126 MHz, $CDCl_3$)** δ 173.89, 170.49, 160.76, 128.94, 128.06, 113.74, 55.35, 43.37, 39.22, 31.70, 29.70, 28.97, 20.04, 13.74.

**4.4.1.2.32**. **N-(tert-butyl)-1-(3,4-dimethoxybenzoyl)piperidine-4-carboxamide** (**A32**)

**$^{1}$H NMR (500 MHz, $CDCl_3$)** δ 6.98 (s, 2H), 6.90 – 6.84 (m, 1H), 5.60 (d, *J* = 45.3 Hz, 1H), 3.86 (s, 6H), 3.24 (s, 2H), 2.95 (s, 2H), 2.33 (d, *J* = 14.9 Hz, 1H), 1.81 (d, *J* = 55.5 Hz, 4H), 1.48 (d, *J* = 14.3 Hz, 2H), 1.38 – 1.27 (m, 4H), 0.93 (t, *J* = 7.3 Hz, 3H). **$^{13}$C NMR (126 MHz, $CDCl_3$)** δ 173.89, 170.42, 150.28, 148.97, 128.23, 119.92, 110.63, 77.30, 77.04, 76.79, 55.99 (d,), 43.36, 39.23, 31.69, 29.69, 28.99, 20.04, 13.74.

**4.4.1.2.33**. **N-(tert-butyl)-1-(4-methoxybenzoyl)piperidine-4-carboxamide** (**A33**)

**$^{1}$H NMR (500 MHz, $CDCl_3$)** δ 7.37 (d, J = 11.4 Hz, 2H), 6.90 (d, J = 6.8 Hz, 2H), 5.28 (d, J = 16.5 Hz, 1H), 3.83 (s, 3H), 2.89 (s, 2H), 2.23 (tt, J = 11.3, 3.9 Hz, 1H), 1.88 – 1.67 (m, 4H), 1.57 (s, 2H), 1.34 (s, 9H). **$^{13}$C NMR (126 MHz, $CDCl_3$)** δ 173.32, 170.50, 128.95, 128.14, 113.72, 55.35, 51.20, 44.07, 29.02, 28.83.

**4.4.1.2.34**. **N-(tert-butyl)-1-(3,4-dimethoxybenzoyl)piperidine-4-carboxamide** (**A34**)

**$^{1}$H NMR (500 MHz, $CDCl_3$)** δ 6.99 – 6.94 (m, 2H), 6.85 (d, J = 8.7 Hz, 1H), 5.28 (s, 1H), 3.89 (d, J = 4.8 Hz, 6H), 2.91 (s, 2H), 2.22 (s, 1H), 1.76 (d, J = 50.7 Hz, 4H), 1.34 (s, 9H), 0.96 – 0.73 (m, 2H). **$^{13}$C NMR (126 MHz, $CDCl_3$)** δ 173.33, 170.43, 150.26, 148.97, 128.32, 119.93, 110.64, 55.99, 51.22, 44.06, 29.70, 28.99, 28.83.

**4.4.1.2.35**. **N,N-diethyl-1-(3-nitrobenzoyl)piperidine-4-carboxamide** (**A35**)

**$^{1}$H NMR (500 MHz, $CDCl_3$)** δ 8.28 – 8.24 (m, 2H), 7.78 – 7.71 (m, 1H), 7.61 (td, *J* = 7.7, 0.9 Hz, 1H), 4.69 (s, 1H), 3.75 (s, 1H), 3.34 (d, *J* = 5.2 Hz, 4H), 3.03 (d, *J* = 93.5 Hz, 2H), 2.73 (dd, *J* = 25.4, 4.1 Hz, 1H), 1.84 (s, 4H), 1.20 (t, *J* = 7.1 Hz, 3H), 1.09 (t, *J* = 7.1 Hz, 3H). **$^{13}$C**

**NMR (126 MHz, $CDCl_3$)** δ 173.07, 167.70, 148.07, 137.61, 132.98, 129.82, 124.45, 122.13, 47.24, 41.85, 40.36, 38.31, 29.10, 28.54, 15.09, 13.09.

**4.4.1.2.36**. **1-(4-bromobenzoyl)-N,N-diethylpiperidine-4-carboxamide** (**A36**)

**$^1$H NMR (500 MHz, $CDCl_3$)** δ 7.53 (d, J = 8.4 Hz, 2H), 7.28 (d, J = 8.4 Hz, 2H), 4.68 (s, 1H), 3.75 (s, 1H), 3.33 (s, 4H), 3.09 – 2.79 (m, 2H), 2.69 (t, J = 14.9 Hz, 1H), 1.83 (s, 4H), 1.20 (t, J = 7.1 Hz, 3H), 1.10 (t, J = 7.1 Hz, 3H). **$^{13}$C NMR (126 MHz, $CDCl_3$)** δ 173.21, 169.38, 134.87, 131.73, 128.65, 123.90, 41.81, 40.32, 38.56, 15.10, 13.10.

**4.4.1.2.37**. **1-(4-chlorobenzoyl)-N,N-diethylpiperidine-4-carboxamide** (**A37**)

**$^1$H NMR (500 MHz, $CDCl_3$)** δ 7.42 – 7.31 (m, 4H), 4.67 (s, 1H), 3.82 (s, 1H), 3.33 (s, 4H), 2.95 (d, J = 90.5 Hz, 2H), 2.69 (d, J = 14.9 Hz, 1H), 1.77 (t, J = 59.0 Hz, 4H), 1.19 (s, 3H), 1.10 (t, J = 7.1 Hz, 3H). **$^{13}$C NMR (126 MHz, $CDCl_3$)** δ 173.24, 169.37, 135.67, 134.38, 128.78, 128.45, 41.82, 40.32, 38.56, 15.09, 13.10.

**4.4.1.2.38**. **N,N-diethyl-1-(3-iodobenzoyl)piperidine-4-carboxamide** (**A38**)

**$^1$H NMR (500 MHz, $CDCl_3$)** δ 7.77 – 7.71 (m, 2H), 7.39 – 7.32 (m, 1H), 7.13 (dd, J = 8.3, 7.7 Hz, 1H), 4.67 (s, 1H), 3.77 (s, 1H), 3.34 (d, J = 4.6 Hz, 4H), 2.95 (d, J = 95.2 Hz, 2H), 2.77 – 2.64 (m, 1H), 1.78 (d, J = 47.2 Hz, 4H), 1.20 (t, J = 7.1 Hz, 3H), 1.10 (t, J = 7.1 Hz, 3H). **$^{13}$C NMR (126 MHz, $CDCl_3$)** δ 173.20, 168.51, 138.60, 138.08, 135.62, 130.22, 125.97, 94.25, 41.82, 40.32, 38.54, 29.11, 15.10, 13.11.

**4.4.1.2.39**. **1-(3-chlorobenzoyl)-N,N-diethylpiperidine-4-carboxamide** (**A39**)

**$^1$H NMR (500 MHz, $CDCl_3$)** δ 7.41 – 7.33 (m, 3H), 7.29 (s, 1H), 4.71 (s, 1H), 3.79 (s, 1H), 3.38 (s, 4H), 2.99 (d, *J* = 98.1 Hz, 2H), 2.73 (d, *J* = 18.9 Hz, 1H), 1.85 (s, 4H), 1.22 (t, *J* = 7.1 Hz, 3H), 1.12 (t, *J* = 7.1 Hz, 3H). **$^{13}$C NMR (126 MHz, $CDCl_3$)** δ 173.21, 168.81, 137.76, 134.57, 129.93, 129.75, 127.03, 124.95, 47.18, 41.82, 40.33, 38.53, 28.87, 28.52 – 27.33, 15.12, 13.10.

**4.4.1.2.40**. **1-(3-bromobenzoyl)-N,N-diethylpiperidine-4-carboxamide** (**A40**)

**$^{1}$H NMR (500 MHz, $CDCl_3$)** δ 7.53 (d, *J* = 7.0 Hz, 2H), 7.32 (d, *J* = 7.6 Hz, 1H), 7.30 – 7.24 (m, 1H), 4.68 (s, 1H), 3.78 (s, 1H), 3.34 (s, 4H), 2.95 (d, *J* = 101.8 Hz, 2H), 2.78 – 2.63 (m, 1H), 1.72 (d, *J* = 109.3 Hz, 4H), 1.20 (t, *J* = 7.1 Hz, 3H), 1.10 (t, *J* = 7.1 Hz, 3H). **$^{13}$C NMR (126 MHz, $CDCl_3$)** δ 173.19, 168.65, 138.02, 132.66, 130.16, 129.88, 125.41, 122.64, 47.17, 41.82, 40.32, 38.53, 28.67, 15.10, 13.10.

**4.4.1.2.41**. **1-(4-chloro-3-nitrobenzoyl)-N,N-diethylpiperidine-4-carboxamide** (**A41**)

**$^{1}$H NMR (500 MHz, $CDCl_3$)** δ 7.93 (d, *J* = 1.8 Hz, 1H), 7.59 (dt, *J* = 8.2, 5.0 Hz, 2H), 4.65 (s, 1H), 3.77 (s, 1H), 3.36 (s, 4H), 3.03 (d, *J* = 100.3 Hz, 2H), 2.73 (s, 1H), 1.77 (d, *J* = 91.9 Hz, 4H), 1.22 (t, *J* = 7.1 Hz, 3H), 1.11 (t, *J* = 7.1 Hz, 3H). **$^{13}$C NMR (126 MHz, $CDCl_3$)** δ 172.97, 166.69, 147.79, 135.80, 132.25, 131.62, 128.36, 124.40, 41.86, 40.38, 38.23, 15.10, 13.10.

**4.4.1.2.42**. **N,N-diethyl-1-(4-nitrobenzoyl)piperidine-4-carboxamide** (**A42**)

**$^{1}$H NMR (500 MHz, $CDCl_3$)** δ 8.32 – 8.23 (m, 2H), 7.63 – 7.53 (m, 2H), 4.71 (d, *J* = 12.8 Hz, 1H), 3.67 (d, *J* = 12.2 Hz, 1H), 3.45 – 3.23 (m, 4H), 3.09 (t, *J* = 12.2 Hz, 1H), 2.92 (s, 1H), 2.72 (t, *J* = 12.7 Hz, 1H), 1.74 (d, *J* = 102.6 Hz, 4H), 1.20 (t, *J* = 7.1 Hz, 3H), 1.10 (t, *J* = 7.1 Hz, 3H). **$^{13}$C NMR (126 MHz, $CDCl_3$)** δ 173.02, 167.99, 148.32, 142.26, 127.90, 123.93, 47.04, 41.85, 40.36, 38.33, 29.65 – 29.20, 28.84, 15.10, 13.09.

**4.4.1.2.43**. **N,N-diethyl-1-(3,4,5-trimethoxybenzoyl)piperidine-4-carboxamide** (**A43**)

**$^{1}$H NMR (500 MHz, $CDCl_3$)** δ 6.61 (s, 2H), 4.68 (s, 1H), 3.84 (d, *J* = 6.6 Hz, 9H), 3.34 (d, *J* = 12.7 Hz, 4H), 2.93 (d, *J* = 44.0 Hz, 2H), 2.70 (d, *J* = 3.9 Hz, 1H), 1.85 (d, *J* = 10.9 Hz, 5H), 1.20 (t, *J* = 7.1 Hz, 3H), 1.10 (t, *J* = 7.1 Hz, 3H). **$^{13}$C NMR (126 MHz, $CDCl_3$)** δ 173.36, 170.21, 153.30, 138.93, 131.44, 103.97, 60.91, 56.24, 41.84, 40.35, 38.72, 15.09, 13.09. **HRMS (ESI):** *m/z* calculated for $C_{20}H_{30}N_2O_5$ $[M+H]^+$: 379.2233; found : 379.2203.

**4.4.1.2.44**. **1-benzoyl-N,N-diethylpiperidine-4-carboxamide** (**A44**)

**$^{1}$H NMR (500 MHz, $CDCl_3$)** δ 7.39 (s, 5H), 4.74 (s, 1H), 3.81 (s, 1H), 3.34 (s, 4H), 2.94 (d, *J* = 70.0 Hz, 2H), 2.68 (s, 1H), 1.84 (s, 4H), 1.20 (t, *J* = 7.1 Hz, 3H), 1.10 (t, *J* = 7.1 Hz, 3H). **$^{13}$C NMR (126 MHz, $CDCl_3$)** δ 173.33, 170.43, 136.11, 129.57, 128.49, 126.86, 47.17, 41.79, 40.28, 38.68, 28.74, 15.09, 13.11. **HRMS (ESI):** *m/z* calculated for $C_{17}H_{24}N_2O_2$ $[M+H]^+$: 289.1916; found : 289.1903.

#### 4.4.1.2.45. N,N-diethyl-1-(4-methoxybenzoyl)piperidine-4-carboxamide (A45)

**$^{1}$H NMR (500 MHz, $CDCl_3$)** δ 7.41 – 7.34 (m, 2H), 6.92 – 6.86 (m, 2H), 4.38 (dd, J = 97.8, 91.0 Hz, 1H), 3.82 (s, 3H), 3.34 (dt, J = 14.2, 7.0 Hz, 4H), 2.93 (s, 2H), 2.68 (dd, J = 18.5, 11.4 Hz, 1H), 1.82 (dt, J = 66.3, 29.2 Hz, 5H), 1.20 (t, J = 7.1 Hz, 3H), 1.10 (t, J = 7.1 Hz, 3H). **$^{13}$C NMR (126 MHz, $CDCl_3$)** δ 173.41, 170.46, 160.67, 128.96, 128.16, 113.69, 77.32, 77.06, 76.81, 55.36, 41.79, 40.28, 38.77, 28.98, 15.09, 13.11.

#### 4.4.1.2.46. 1-(3,4-dimethoxybenzoyl)-N,N-diethylpiperidine-4-carboxamide (A46)

**$^{1}$H NMR (500 MHz, $CDCl_3$)** δ 7.02 – 6.94 (m, 2H), 6.84 (d, *J* = 8.3 Hz, 1H), 4.62 (s, 1H), 3.89 (d, *J* = 3.3 Hz, 6H), 3.35 (dq, *J* = 14.0, 6.9 Hz, 4H), 2.95 (s, 2H), 2.76 – 2.62 (m, 1H), 2.10 – 1.55 (m, 5H), 1.20 (t, *J* = 7.1 Hz, 3H), 1.10 (t, *J* = 7.1 Hz, 3H). **$^{13}$C NMR (126 MHz, $CDCl_3$)** δ 173.39, 170.38, 150.15, 148.89, 128.34, 119.89, 110.54, 77.32, 55.98, 41.80, 40.30, 38.77, 28.92, 15.09 (d,), 13.10.

#### 4.4.1.2.47. 1-(3-nitrobenzoyl)-N-propylpiperidine-4-carboxamide (A47)

**$^{1}$H NMR (500 MHz, $CDCl_3$)** δ 8.32 – 8.22 (m, 2H), 7.77 – 7.70 (m, 1H), 7.62 (t, *J* = 7.9 Hz, 1H), 5.58 (s, 1H), 4.68 (s, 1H), 3.71 (s, 1H), 3.22 (t, *J* = 10.0 Hz, 2H), 3.02 (d, *J* = 88.9 Hz, 2H), 2.37 (d, *J* = 30.1 Hz, 1H), 1.83 (t, *J* = 55.2 Hz, 4H), 1.51 (dt, *J* = 14.6, 7.3 Hz, 2H), 0.91 (t, *J* = 7.4 Hz, 3H). **$^{13}$C NMR (126 MHz, $CDCl_3$)** δ 173.54, 167.74, 148.08, 137.54, 132.97, 129.86, 124.52, 122.12, 77.32, 77.06, 76.81, 47.25, 43.03, 41.24, 29.15, 22.90, 11.35.

#### 4.4.1.2.48. 1-(4-bromobenzoyl)-N-propylpiperidine-4-carboxamide (A48)

**$^{1}$H NMR (500 MHz, $CDCl_3$)** δ 7.58 – 7.54 (m, 2H), 7.32 – 7.27 (m, 2H), 5.62 (s, 1H), 4.66 (s, 1H), 3.80 (s, 1H), 3.23 (t, J = 12.9 Hz, 2H), 2.96 (d, J = 89.2 Hz, 2H), 2.45 – 2.24 (m, 1H), 1.88 (d, J = 93.7 Hz, 4H), 1.62 – 1.45 (m, 2H), 0.93 (t, J = 7.4 Hz, 3H). **$^{13}$C NMR (126 MHz, $CDCl_3$)** δ 173.74, 169.42, 134.76, 131.77, 128.63, 124.00, 43.23, 41.19, 22.87, 11.35.

**4.4.1.2.49**. **1-(4-nitrobenzoyl)-N-propylpiperidine-4-carboxamide** (**A49**)

**$^{1}$H NMR (500 MHz, $CDCl_3$)** δ 8.27 (d, J = 8.7 Hz, 2H), 7.60 – 7.53 (m, 2H), 5.55 (s, 1H), 4.68 (d, J = 11.1 Hz, 1H), 3.66 (d, J = 11.5 Hz, 1H), 3.22 (q, J = 6.3 Hz, 2H), 2.99 (d, J = 75.8 Hz, 2H), 2.42 – 2.27 (m, 1H), 2.08 – 1.71 (m, 4H), 1.60 – 1.46 (m, 2H), 0.91 (t, J = 7.4 Hz, 3H**).** **$^{13}$C NMR (126 MHz, $CDCl_3$)** δ 173.51, 168.03, 148.35, 142.16, 127.90, 123.96, 77.31, 77.06, 76.80, 47.06, 43.02, 41.73, 41.22, 28.84, 22.83, 11.34.

**4.4.1.2.50**. **N-propyl-1-(3,4,5-trimethoxybenzoyl)piperidine-4-carboxamide** (**A50**)

**$^{1}$H NMR (500 MHz, $CDCl_3$)** δ 6.60 (s, 2H), 5.57 (s, 1H), 4.66 (s, 1H), 3.85 (d, J = 5.3 Hz, 9H), 3.22 (d, J = 26.1 Hz, 2H), 2.98 (s, 2H), 2.45 – 2.25 (m, 1H), 1.78 (d, J = 19.6 Hz, 4H), 1.55 – 1.46 (m, 2H), 1.30 – 1.09 (m, 1H), 0.91 (t, J = 7.4 Hz, 3H). **$^{13}$C NMR (126 MHz, $CDCl_3$)** δ 173.87, 170.23, 153.32, 139.02, 131.36, 104.01, 77.31, 77.06, 76.80, 60.91, 56.25, 43.38, 41.19, 22.87, 11.35.

**4.4.1.2.51**. **1-(4-methoxybenzoyl)-N-propylpiperidine-4-carboxamide** (**A51**)

**$^{1}$H NMR (500 MHz, $CDCl_3$)** δ 7.36 (d, J = 2.0 Hz, 1H), 7.35 – 7.34 (m, 1H), 6.89 (d, J = 8.8 Hz, 2H), 5.72 (s, 1H), 4.58 (s, 1H), 3.82 (s, 4H), 3.24 – 3.15 (m, 2H), 2.92 (s, 2H), 2.32 (t, J = 11.4 Hz, 1H), 1.89 – 1.64 (m, 4H), 1.57 – 1.42 (m, 2H), 0.90 (t, J = 7.4 Hz, 3H). **$^{13}$C NMR (126 MHz, $CDCl_3$)** δ 173.97, 170.49, 160.74, 128.94, 128.02, 113.73, 55.37, 43.39, 41.15, 28.97, 23.17 – 22.56, 11.36.

**4.4.1.2.52**. **1-(3,4-dimethoxybenzoyl)-N-propylpiperidine-4-carboxamide** (**A52**)

**$^{1}$H NMR (500 MHz, $CDCl_3$)** δ 6.96 (dq, J = 3.8, 1.9 Hz, 2H), 6.84 (d, J = 8.7 Hz, 1H), 5.62 (s, 1H), 4.60 (s, 1H), 3.89 (d, J = 4.5 Hz, 6H), 3.21 (dd, J = 11.8, 5.9 Hz, 2H), 2.92 (s, 2H), 2.34 (d, J = 7.0 Hz, 2H), 1.80 (d, J = 44.4 Hz, 4H), 1.49 (dd, J = 14.5, 7.3 Hz, 2H), 0.90 (t, J = 7.4 Hz, 3H). **$^{13}$C NMR (126 MHz, $CDCl_3$)** δ 173.95, 170.43, 150.23, 148.93, 128.19, 119.90, 110.62, 55.99, 43.43, 41.18, 28.99, 22.83, 11.35.

### 4.4.2. In Vitro Assay

#### 4.4.2.1. Production and purification of recombinant human ChAT protein

Recombinant human ChAT protein was produced and purified by the Protein Science Facility (PSF) at Karolinska Institute/SciLifeLab (http://ki.se/psf), as described before (10). The purity of protein was determined using sodium dodecyl sulfate polyacrylamide gel (SDS-PAGE) stained with Coomassie blue dye. The total protein concentration was measured using BioRad DC protein Assay (BioRad). The storage buffer for the protein was 20 mM HEPES buffer, pH 7.5, containing 300 mM NaCl, 0.5 mM TCEP. The protein was diluted in the storage buffer to a concentration of 212 μg/mL. The diluted enzyme solution was then aliquoted (10μL/tube), frozen on dry ice, and stored at -20°C.

#### 4.4.2.2. In vitro fluorometric ChAT activity inhibition assay

The synthesized compounds were subjected to *in-vitro* ChAT activity inhibition assay using our in-house developed high throughput fluorometric method, utilizing human recombinant ChAT (rChAT) protein (9). The required reagents choline chloride, acetyl coenzyme-A (ACoA, A2181) and 7-Diethylamino-3-(4-maleimidophenyl)-4-methylcoumarin (CPM) for carrying out the study were purchased from Sigma-Aldrich (St. Louis, MO, USA).

The ChAT assay was run in 384-well plates (Greiner Bio-One Item-No. 781209). The dilution buffer was 20mM HEPES, pH 7.4 (containing 150 mM NaCl, 1.0 mM EDTA, 0.05% (v/v) Triton X-100). First, 20 μL/well of a 600μM choline chloride solution (final concentration, $C_f$, 150 μM), and then 20 μL/well of a 0.212μg/ml of the recombinant ChAT ($C_f$ = 0.053μg/mL)

was added. Thereafter, 20µL/well of 400µM of different hit compounds were added to the wells, and incubated for ~30 minutes at room temperature under gentle orbital shaking (200rpm). Finally, the reaction was started by adding 20µL of a cocktail-A [containing 54µM ACoA ($C_f$ = 13.3 µM) and 60 µM CPM ($C_f$ = 15 µM)] was to each well. Immediately after adding the cocktail-A, the changes in fluorescence were monitored continuously at 3 minutes intervals for 30 minutes using a microplate spectrophotometer reader (Infinite M1000, Tecan). The excitation and emission wavelengths were 390 nm and 479 nm, respectively. Each compound was applied in six replicates. On each 384-wells plate, several enzyme wells without any hit compounds but the vehicle were also included to serve as reference enzyme control wells. The vehicle was the compound dilution buffer containing the same amount of DMSO as the compound's wells. Negative controls (or blanks) were wells without enzyme. The total volume in all wells were 80µL. The percentage inhibition for each compound was calculated based on the enzyme control value as a reference (100% activity). Based on the initial screening we selected the two most potent compounds that inhibited ChAT selectively for the enzyme inhibition kinetic studies.

**4.4.2.3. In vitro colorimetric AChE and BChE activity inhibition assay**

An in-house high throughput assay for the enzymatic activity of BChE and AChE was designed using a modified version of Ellman's colorimetric assay. The reagents, butyrylthiocholine iodide (BTC), acetylthiocholine iodide (ATC), and 5,5′-dithiobis (2-nitrobenzoic acid) (DTNB), were purchased from Sigma-Aldrich (St. Louis, MO, USA). The buffer system for AChE and BChE assays was sodium/potassium phosphate buffer (50mM, pH 7.4).

Briefly, for screening of compounds against BChE, 20 µL/well of a 1:100 diluted solution of a pooled human plasma (final dilution 1/400) was added to the wells of a 384 well plate (a flatbottom transparent plate). For screening against AChE, 20 µL/well of a 1:768 diluted ($C_f$ = 3.5 ng/mL) solution purified recombinant human AChE protein (Sigma, Cat no. C1682) was

used. Then 20 µL/wells of a 400µM hit compounds solution ($C_f$ = 100µM) was added to the assigned wells (six replicates/compound), followed by adding 20µL/well of a 1.6 mM freshly prepared solution of DTNB ($C_f$ = 0,4 mM) to all wells. The plate was incubated at RT for ~30 min. On each 384-wells plate, several enzyme wells without any hit compounds but the vehicle were also included to serve as reference enzyme control wells. The vehicle contained the same amount of DMSO as the compound's wells. Negative controls (or blanks) were wells without enzyme. Lastly, 20 µL of a 4.0 mM BTC solution ($C_f$ = 1 mM) or a 2.0 mM ATC ($C_f$ = 0.5 mM) was added to each well, and the changes in absorbance were continuously monitored at 412 nm wavelength for 10 min with 1 min interval, using a microplate spectrophotometer reader (Infinite M1000, Tecan). The rate of the enzyme activity was determined from the linear part of the kinetic reaction curves as ΔOD/time. The total volume in all wells were 80µL. The percentage inhibition for each compound was calculated based on the enzyme control value as a reference (100% activity).

**4.4.2.4. Enzyme inhibition kinetics for determination of $K_i$, $IC_{50}$, and mode of action of hits compounds**

Likewise, an identical protocol as inhibition assay was performed, a 2-fold dilution series of the compound is dispensed to 384 well plate, starting with a stock concentration of 50 mM. The compound is then diluted to five different concentrations of dilution series ranging from 100 to 6.25 µM for the top selected compound A1. Followed by preparing and adding a 2-fold dilution series of choline to each well. The final concentrations of choline range from 320 µM to 0 µM. ChAT enzyme solution is added to each well resulting in a final concentration of 0.053 µg/mL in each well. The 384 well plate is incubated at room temperature with 200 rpm orbital shaking for 30 minutes. The spectrophotometer is set up for read fluorescence intensity reading at 3-minute intervals. The excitation wavelength is set at 390 nm and the emission is measured at 479 nm. Finally, a 4-fold fluorescent detection reagent solution, which is prepared by mixing

dilution buffer, 1 mM ACoA, and CPM stock solution was added (20 µL/well), resulting in a final concentration of 13.33 µM, 60 µM, and 15 µM, respectively. The rate of enzyme activity (RFU/hr/53ng rhChAT) was calculated and processed using the GraphPad Prism 7 analysis software(11). The inhibitory constant ($K_i$) values were determined from the dose-response curve along with the half-maximal inhibitory concentration ($IC_{50}$) calculated by plotting the percentage enzyme activity vs. the log of the compounds concentrations and fitting it with the nonlinear regression enzyme kinetics-inhibition function. The Michaelis-Menten constant ($K_m$) and maximal velocity ($V_{max}$) values were also obtained from the substrate-velocity curve by fitting the data with non-linear regression Michaelis-Menten kinetic function. These values were then used for making the Lineweaver-Burk plot and was fitted using the linear regression function.

#### 4.4.2.5. In Vitro Cytotoxicity Assay

MTT assay was performed for the top performing compound A1 to determine the *in vitro* cellular toxicity. Human neuroblastoma SH-SY5Y cells (ATCC, CRL-2266) were cultured at 37°C in a humidified environment with 5% $CO_2$ in Dulbecco's Modified Eagle's medium (DMEM) with 10% fetal bovine serum (FBS) in 96-well plate to obtain 70–80% confluency. The cells were incubated with 10 µM and 50 µM compounds in sextuplicate for 24 h at 37 °C. Cells treated with 0.25% DMSO were used as controls. At the end of the treatment, 20 µL of MTT (5 mg/mL in Phosphate buffer saline pH 7.4) was added to each well and incubated for an additional 4 h at 37 °C. The media was then removed from the plate and 200 µL of DMSO was added to dissolve the violet formazan crystals. Finally, the absorbance was measured at 570 nm with a reference wavelength of 630 nm on CLARIOstar Plus microplate reader (BMG Labtech) with shaking before the reading. The percentage viability was calculated taking 0.25% DMSO control as 100 percent and represented as mean ± SD.

### 4.4.3. In Vivo Studies of Compound A1 in Sprague Dawley rats

**4.4.3.1. Experimental animals**: Sprague Dawley Rats (200-250 gm) equally male and female were used in the study. Animals were housed in five per cage in standard housing conditions; temperature 21 ± 2°C; 12-hour light-dark cycle. Animals were provided with standard laboratory food *ad-libitum* and sterile water. All the animals were randomly assigned to the different experimental groups (n=6/group). All experiments and methods used in this research followed the recommendations set by the Committee for the Control and Supervision of Animal Experiments, under the Ministry of Environment, Forests and Climate Change, India. We also received approval from the University's Central Animal Ethics Committee (IIT, BHU, Varanasi, India) with reference IAFC Approval Number: IIT(BHU)/IAEC/2012/005 and IIT(BHU)/IAEC/2012/006.

#### 4.4.3.2. Motor coordination

The rotarod test was performed as per previously published protocols with minor modifications. Mice were placed in the testing room for at least 1hr before testing to minimize the effects of stress on behavior during testing. Animals from the same cage are placed in separate lanes on rod rotating at 5 rpm such that animals may walk forward to keep balance. After 60 s on the rod, animals are returned to their home cage. The procedure is repeated for a total of three trials separated by 10 min inter-trial intervals. The apparatus is set to accelerate from 4 to 40 rpm in 300 s, and animals from the same cage are placed in separate lanes on the rod initially rotating at 4 rpm. Trial begins when acceleration is started and ends when the animal falls off the rotating rod. The procedure is repeated for a total of three trials separated by 15 min intertrial intervals.

#### 4.4.3.3. In vivo pharmacokinetics

The study was done according to the approved study protocol (IIT(BHU)/IAEC/2023/005). Animals were divided into six groups with n=6/group, where each group consisted 3 male and

female each. Two routes of administration were selected intravenous (i.v.) injection through tail vein and per oral (p.o.) through oral gavage, at a dosage of 1 mg/kg, 5 mg/kg and 10 mg/kg each. Before administration, the hit compound A1 was prepared by dissolving in saline using 1% DMSO. Blood samples were withdrawn and collected from the retro-orbital route at specific time intervals of 0, 0.5, 1, 2, 4, 8, 12 and 24 hours, in heparinized micro-centrifuge tubes and were immediately processed for plasma separation using a centrifuge at 7000 rpm for 5 min at 4°C. The supernatant plasma was carefully separated by the help of micropipette and was further stored at -80°C for further processing in the HPLC. Time zero hour (0 hour) was referred to as the control blank for the study.

#### 4.4.3.4. In vivo brain kinetics

In a separate study brain kinetics was performed on 18 rats, where each rats received the highest dosage of 10 mg/kg body weight of compound A1. Three rats were sacrificed at each given time point of 0, 0.5, 1, 2, 6 and 12 hours and their brains were extracted. For homogenization process, the brains were weighed accurately and homogenized with 1:5 w/v of 50% v/v aqueous acetonitrile. The brain tissue samples were then centrifuged at 7000 rpm for 15 min at 4°C, and the supernatant was collected. The resultant samples of brain homogenate were stored at−80°C until further analysis through HPLC. Time zero hour (0 hour) was referred to as the control blank for the study.

### 4.4.4. Solubility and percentage purity assay

Solubility study was performed as reported earlier. Initially making a primary stock solution of 10 mM of compound A1 in an organic solvent (DMSO), followed by taking 50 µL of the 10 mM DMSO stock and adding it to a 950 µL of 1 M phosphate buffer saline (PBS) with a pH of 7.4. The resultant solution was set for 1.5 hours of mixing. The resultant solution was centrifuged and filtered using 0.22 µm nylon syringe filter and was quantified using RP-HPLC

method. Calibration curve was made for the compound by taking 7 serial dilutions as follows, 200 µM, 100 µM. 50 µM. 25 µM, 12.5 µM, 6.25 µM and 3.125 µM, and the $R^2$ value for the compound A1 was found to be 0.9976. The percentage purity calculations were carried out using the 100 µM sample concentrations. HPLC Instrument used: Agilent 2004, Method for A1: Solvent system used Acetonitrile = 0-70%: Water = 100-30% for the initial 2 minutes at gradient followed by isocratic run for 9 minutes. Flow rate was set to 0.8 ml/min. Absorbance was recorded at 250 nm. Sample volume for each injection was 20 µl, Column Specification: Poroshell 123, EC C18 4 µm, 4.6*150 mm.

### 4.4.5. Computational Details

#### 4.4.5.1. Molecular Docking

To investigate the molecular interactions of the synthesized compounds A1, we performed the molecular docking study using AutoDock Vina (12) against ChAT protein (PDB id: 2FY3) (13). The structure of the compound A1 and α-NETA (standard, known ChAT inhibitor) was drawn using ChemDraw Ultra (14) and were saved as .mol file which was further processed using Chem 3D Pro 12.0 (15) to energy minimize and save as .pdb format, followed by converting the structure to .pdbqt using AutoDock Tools 1.5.7. (12) Likewise, the ChAT protein was pre-processed and all the water and ion molecules were removed and all the ligands were removed, followed by addition of hydrogens, assigning AD4 type atoms and kollman charges were added and was saved as .pdbqt. The grid box was prepared and was set to 6.333, -3.639, 67.306 coordinates from the center for X, Y, Z coordinates respectively encompassing the ChAT binding tunnel and the box size was set to 26X26X26 Å in dimension. Finally, the docking was carried out and the interaction diagram was obtained from Discovery Studio 2021 (16).

### 4.4.5.2. Molecular Dynamics

Molecular dynamics simulation was performed for the two top performing hits with the help of GROMACS 2020 (17, 18) and CHARMM36M force field (19) was used. The redocked pose obtained from the Glide XP docking protocol was taken as the starting frame for the simulation. System preparation was performed as per the protocol mentioned in our previous article. Briefly, the complexes were solvated in a cubic box and TIP3 mode used as a water model for the system, with a 1.0 nm distance from each side of the complex and between the solvation box edges. 0.15 molar $Na^+$ and $Cl^-$ ions was added to neutralize the system. The built system was then subjected to energy minimization by utilizing the steepest descent algorithm such that the maximum forces become less than 1000 kJ/mol/nm in order to obtain a decent starting structure for the simulation production run. Position restraints were set for the equilibration step by constant moles, volume and temperature in the canonical ensemble (NVT) and isothermal-isobaric ensemble (NPT), each for 2ns so as to prevent distortions that can result in blow up of the system during the production run due to the lack of stability. The system condition was kept at 310.15 K temperature applying the V-rescale temperature coupling and pressure was maintained at 1 bar using the Parrinello–Rahman pressure coupling with a coupling constant of 0.1 picosecond for the temperature setting and 2 picoseconds for the pressure setting. Particle mesh Ewald (PME) method was used to calculate the long-range electrostatic interactions and van der Waals interactions, the cut-off for short-range van der Waals was set to 1 nm (20). LINCS algorithm was used for setting constraints on the bonds and the time step was kept at 0.002 ps for the simulation run (21). Finally, a 200 ns production run was initiated under the periodic boundary conditions. The obtained trajectories were further analyzed for its RMSD, RMSF, RoG, SASA, HBN, hydrogen bond distance (HBD), PCA and FEL.

## 4.5. Conclusion

In this chapter we have synthesized a total of fifty-two compounds and have characterized by NMR and HRMS techniques. All the synthesized compounds were evaluated for their inhibitory potential against ChAT enzyme in vitro. The in vitro screening assay revealed that many compounds inhibited ChAT with over 50% inhibition, therefore, we further screened the compounds for its off-target effects on AChE and BuChE where we observed various compounds selectively inhibited ChAT having negligible off-target binding, Among the series compound A1 emerged out to be the best performing compound which was carried forward for detailed in-vitro evaluation and the $IC_{50}$ and $K_i$ values were determined which was found to be 31.08 and 21.36 µM. Also, the cytotoxicity tests on SHSY5Y cell lines showed that our compound A1 was non-toxic and have no effect on the cell viability. Further the compound A1 was tested in vivo for its parameter and brain permeability, which suggested that it had optimal pharmacokinetics and have a good brain permeability reaching the target tissue effectively. Additionally, molecular docking and dynamic studies provided crucial insight into the mode of binding and complex formation process with the ChAT binding tunnel, it was observed that the Nitro group of the phenyl ring of the compound A1 interacted with the HIS324 residue. In summary the present study underscores the potential of A1 as a promising lead compound for further research to be developed as potential PET imaging biomarker for ChAT in order to track and monitor the cholinergic neuronal health. The findings also indicate the potential of piperidine ring system, holding huge potential that are to be further explored.

## 4.6. References

1. Scheltens P, De Strooper B, Kivipelto M, Holstege H, Chételat G, Teunissen CE, et al. Alzheimer's disease. The Lancet. 2021;397(10284):1577-90.
2. Jia J, Ning Y, Chen M, Wang S, Yang H, Li F, et al. Biomarker changes during 20 years preceding Alzheimer's disease. New England Journal of Medicine. 2024;390(8):712-22.
3. Vardanyan R. Piperidine-based drug discovery: Elsevier; 2017.

4. Frolov NA, Vereshchagin AN. Piperidine derivatives: recent advances in synthesis and pharmacological applications. International Journal of Molecular Sciences. 2023;24(3):2937.
5. Abdelshaheed MM, Fawzy IM, El-Subbagh HI, Youssef KM. Piperidine nucleus in the field of drug discovery. Future Journal of Pharmaceutical Sciences. 2021;7:1-11.
6. Ahmad M. Donepezil: A review of the recent structural modifications and their impact on anti-Alzheimer activity. Brazilian Journal of Pharmaceutical Sciences. 2020;56:e18325.
7. Waldemar G, Gauthier S, Jones R, Wilkinson D, Cummings J, Lopez O, et al. Effect of donepezil on emergence of apathy in mild to moderate Alzheimer's disease. International journal of geriatric psychiatry. 2011;26(2):150-7.
8. Therriault J, Schindler SE, Salvadó G, Pascoal TA, Benedet AL, Ashton NJ, et al. Biomarker-based staging of Alzheimer disease: rationale and clinical applications. Nature Reviews Neurology. 2024;20(4):232-44.
9. Kumar R, Kumar A, Långström B, Darreh-Shori T. Discovery of novel choline acetyltransferase inhibitors using structure-based virtual screening. Scientific reports. 2017;7(1):16287.
10. Kumar R, Kumar A, Nordberg A, Långström B, Darreh-Shori T. Proton pump inhibitors act with unprecedented potencies as inhibitors of the acetylcholine biosynthesizing enzyme—a plausible missing link for their association with incidence of dementia. Alzheimer's & Dementia. 2020;16(7):1031-42.
11. Swift ML. GraphPad prism, data analysis, and scientific graphing. Journal of chemical information and computer sciences. 1997;37(2):411-2.
12. Huey R, Morris GM, Forli S. Using AutoDock 4 and AutoDock vina with AutoDockTools: a tutorial. The Scripps Research Institute Molecular Graphics Laboratory. 2012;10550(92037):1000.
13. Kim A-R, Rylett RJ, Shilton BH. Substrate binding and catalytic mechanism of human choline acetyltransferase. Biochemistry. 2006;45(49):14621-31.
14. Cousins KR. ChemDraw Ultra 9.0. CambridgeSoft, 100 CambridgePark Drive, Cambridge, MA 02140. www. cambridgesoft. com. See Web site for pricing options. ACS Publications; 2005.
15. Hinchliffe A. CS Chem3D Pro (Version 3.2 for Windows). Wiley Online Library; 1996.
16. Jejurikar BL, Rohane SH. Drug designing in discovery studio. 2021.
17. Van Der Spoel D, Lindahl E, Hess B, Groenhof G, Mark AE, Berendsen HJ. GROMACS: fast, flexible, and free. Journal of computational chemistry. 2005;26(16):1701-18.
18. Abraham MJ, Murtola T, Schulz R, Páll S, Smith JC, Hess B, et al. GROMACS: High performance molecular simulations through multi-level parallelism from laptops to supercomputers. SoftwareX. 2015;1:19-25.
19. Huang J, Rauscher S, Nawrocki G, Ran T, Feig M, De Groot BL, et al. CHARMM36m: an improved force field for folded and intrinsically disordered proteins. Nature methods. 2017;14(1):71-3.
20. Cheatham TI, Miller J, Fox T, Darden T, Kollman P. Molecular dynamics simulations on solvated biomolecular systems: the particle mesh Ewald method leads to stable trajectories of DNA, RNA, and proteins. Journal of the American Chemical Society. 1995;117(14):4193-4.
21. Hess B, Bekker H, Berendsen HJ, Fraaije JG. LINCS: a linear constraint solver for molecular simulations. Journal of computational chemistry. 1997;18(12):1463-72.